DESIGN AND CHARACTERIZATION OF A UHF DIPLEXER/ANTENNA COMBINATION

BY

ZHIYUAN ZHENG

THESIS

Submitted in partial fulfillment of the requirements
for the degree of Master of Science in Electrical and Computer Engineering
in the Graduate College of the
University of Illinois at Urbana-Champaign, 2016

Urbana, Illinois

Adviser:

Dr. Serge Minin

ABSTRACT

Wireless communication systems are important in modern day life. Applications of wireless communication systems are used everywhere around the world, such as cell phones, wireless entertainments, satellites and navigation services. Because of the high volume usage of various wireless signals' spectra, it is desired to design systems that can accept the frequencies of multiple signals. A combination of antenna and diplexers can achieve such functionality. With antennas operating in dual frequency and diplexers which separate the signals, dual-frequency signals can be effectively transferred through the wireless communication systems simultaneously.

In this thesis, we simulate and characterize the behavior of antenna and diplexer functioning in dual frequency. For the antenna, a mathematical analysis and a circuit model analysis were conducted to replicate its behavior. On the other hand, several circuit designs and simulations have been performed for diplexers. Moreover, an initial implementation of a single-order diplexer is also discussed. After the measurement, we found reasonable results for the functionality of a single-order diplexer. We believe that this first step gives us a correct route to our final implementation goal.

In the future, more implementation tasks can also be discussed. In addition to the implementation of a first-order diplexer, higher-order diplexers constructed on printed circuited board (PCB) can also be developed. Moreover, an implementation of a combinational matching network construction between antenna and diplexer can also be discussed.

To my parents, for their love and support.

ACKNOWLEDGMENTS

Foremost, I would like to express my sincere gratitude to my advisor, Serge Minin, for the continuous support of my graduate research. His guidance helped me to overcome enormous difficulties encountered during the research. I could not have imagined having a better advisor and mentor for my graduate study.

Besides my advisor, I would like to thank Professor Steve Franke for his patience, motivation, enthusiasm, and immense knowledge. He answered all my questions patiently and thoughtfully despite his busy schedule.

TABLE OF CONTENTS

CHAPTER 1 INTRODUCTION 1
1.1 Motivation 1
1.2 Overview 1

CHAPTER 2 ANTENNA MODEL AND DESIGN 3
2.1 Introduction 3
2.2 Strip Dipole 3
2.3 Cross Dipole Antenna 8
2.4 Antenna Equivalent Circuit Model 11

CHAPTER 3 DIPLEXER MODEL AND DESIGN 18
3.1 Introduction 18
3.2 Filter Basic 18
3.3 Diplexer Design 30

CHAPTER 4 COMBINATION OF ANTENNA AND DIPLEXER . . 36
4.1 Introduction 36
4.2 Matching Network Basics 36
4.3 Matching Network Design between Diplexer and Cross Dipole Antenna 39

CHAPTER 5 IMPLEMENTATION AND FABRICATION 41
5.1 Introduction 41
5.2 Microstrip Transmission Line Characterization 41
5.3 Filter Implementation 44

CHAPTER 6 CONCLUSION 52
6.1 Conclusion 52
6.2 Future Work 52

APPENDIX A TEM-MODE TRANSMISSION LINE 54

APPENDIX B CALIBRATION 56
B.1 SOLT vs. TRL 57

REFERENCES 59

CHAPTER 1

INTRODUCTION

1.1 Motivation

The importance of wireless has been emphasized for at least two decades. Applications of wireless communication systems have been evolving from the original voice service such as first-generation analog phones to high-data-rate-applications such as Internet of Things. Because of the large variety in wireless communication applications in different operating frequencies, modules that can combine and distinguish different signal frequencies are desired, such as antennas, diplexers, duplexers, circulators, etc. Although such technology in microwave frequency range (cellular, wifi, Bluetooth) has matured, improvements are still required for the applications in ultra high frequency (where some amateur satellites lie). The materials for designing antennas and diplexers are usually expensive. Therefore, in this thesis, we attempt to design an antenna and a diplexer using materials that are easy to access (such as FR4, copper, etc.). We believe this approach can benefit researchers later who are interested in designing wireless communication systems in ultra high frequency (UHF).

1.2 Overview

For this master's thesis, the communication system uses two radios and one single antenna. The conceptual diagram of the hardware is shown in Figure 1.1.

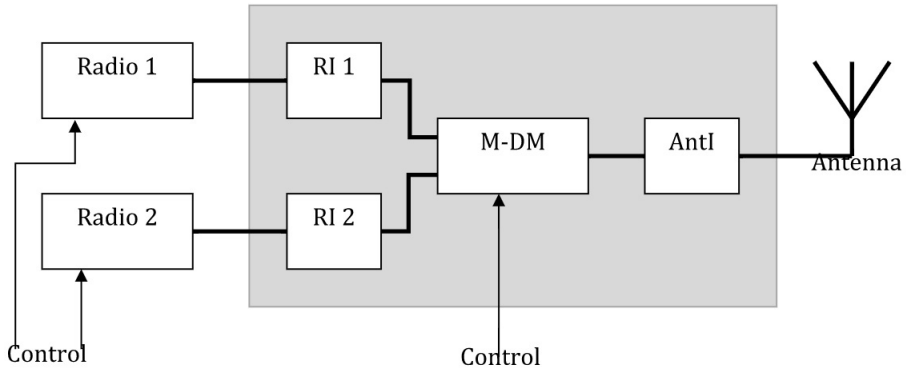

Figure 1.1: Conceptual diagram of radio system

In the radio system, the antenna is a four-element cross-dipole, which is retained on the -Z face of the satellite. The antenna is secured during launch using a nylon monofilament which is stretched across thermal knives located on the +X, -X, +Y, and -Z faces of the satellite [1]. Moreover, Radio 1 is a HAM radio operating at 420 MHz, and it is mostly used for telemetry and can be accessed by various ground stations. Radio 2 is a high-data-rate radio operating at 470 MHz, and it will download the science data to a designated ground station.

The RF interface module, which is highlighted in Figure 1.1, allows two transceiver radios to use a single antenna. It is convenient to break up the interface design into four parts: the first radio interface (RI1), the second radio interface (RI2), the multiplexer/demultiplexer (M-DM) for the two radios, and the antenna interface (AntI).

For the radio interface, the ideal configuration would be a diplexer, connecting Radio 1 and Radio 2 signals to the antenna without any loss, reflection, or crosstalk. It would also perfectly separate the two bands received by the antenna. Although, due to the technology limitation, solid-state high-power switches were selected as a leading design concept [1], we still believe the interface can be realized using a passive diplexer.

The radio interface and antenna interface blocks of the RF interface would ensure proper matching of the radios to the switch and the antenna. These blocks would be constructed on a printed circuit board with discrete and transmission line components. The design will be based on the scattering parameter measurements and will be iterated experimentally to achieve maximum power transfer.

CHAPTER 2

ANTENNA MODEL AND DESIGN

2.1 Introduction

In a typical wireless communication system, an antenna is an electrical component that can transform radio waves into electric power, and vice versa. Usually the antenna is used in both transmitting mode and receiving mode. In reception, an antenna always intercepts some amount of power from an electromagnetic wave and then produces a tiny voltage at its terminals, which is applied to a receiver to be amplified.

There are various kinds of antennas being used in contemporary applications; the most widely used is the dipole antenna. A dipole antenna is composed of two symmetrical radiators such as metal rods or wires, with one side of a balanced feedline from the transmitter or receiver attached as the antenna feeds [2]. Among different kinds of dipole antennas, a half-wave dipole is the most commonly used. A half-wave dipole antenna has two collinear elements, each a quarter wavelength long. In this chapter, we will discuss two types of antennas which we have used in our thesis.

2.2 Strip Dipole

Strip dipole antennas are more convenient than wire dipole antennas in cylindrical forms. Strip dipoles can be fabricated on dielectric substrates and used in linear and planar arrays at microwave frequencies [3]. A printed strip dipole antenna of width W can be modeled as a cylindrical dipole antenna with a radius $r = w/4$ [4], as illustrated in Figure 2.1.

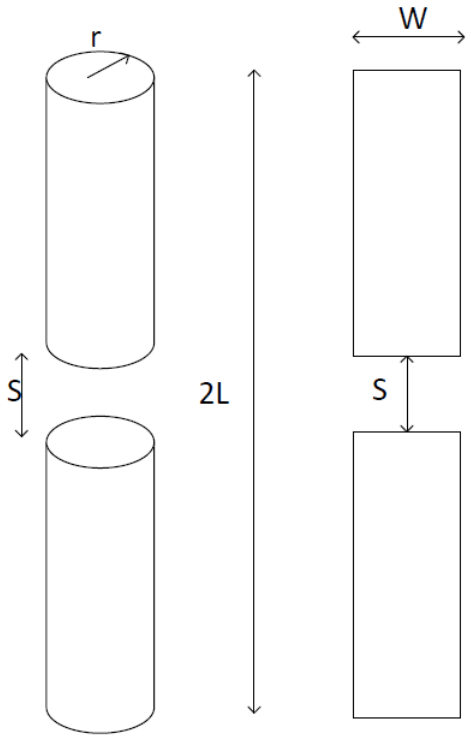

Figure 2.1: Model for cylindrical and strip dipole

One of our primary goals in wireless communication systems design is to deliver sufficient power to the RF front-end modules after it is received by the antenna. In order to accomplish this goal, a matched diplexer must be designed appropriately.

Matching the diplexer with the antenna means that the impedance of the diplexer should be conjugately matched with antenna. Therefore, we need to calculate the self-impedance of the antenna. In the rest of this chapter, two methods (analytical and equivalent circuit) will be evaluated. The analytical way of calculating self-impedance of a strip-dipole antenna is explained in [3]. In this paper, the authors demonstrate a novel way to calculate input impedance of a center-fed strip dipole based on the King-Middleton second-order solution discuss in [5]. The King-Middleton method is a set of equations derived by R. W. P. King and authors to calculate the impedance of cylindrical antennas based on the electrical length, radius and wavelength of the antennas. From what we discussed earlier, a strip-dipole can be modeled as a cylindrical dipole for $r = w/4$, where r is the cylindrical radius and w is the width for strip dipole. The King-Middleton method can be represented

as (2.1):

$$R(kl, \frac{a}{\lambda}) = \sum_{m=0}^{4} \sum_{n=0}^{4} a_{mn} (kl)^m (\frac{a}{\lambda})^n \tag{2.1}$$

$$X(kl, \frac{a}{\lambda}) = \sum_{m=0}^{4} \sum_{n=0}^{4} b_{mn} (kl)^m (\frac{a}{\lambda})^n \tag{2.2}$$

where k is the propagation constant defined as $k = \frac{2\pi}{\lambda}$, l is half of the dipole length, and a is the radius of the cylinder.

The coefficients a_{mn} and b_{mn} can be found in Table 2.1 and Table 2.2:

Table 2.1: The coefficient table of a_{mn}

m \ n	0	1	2	3	4
0	1.8115e2	3.91e5	-4.2139e7	1.5370e9	6.1253e10
1	-6.3433e2	-1.0232e6	-9.5644e7	-1.6606e9	-2.8222e11
2	8.3517e2	1.0004e6	-7.7690e7	-8.8929e8	4.0597e11
3	-4.6128e2	-4.3749e5	2.7195e7	1.3870e9	-2.2850e11
4	-1.0222e2	7.3332e4	-3.6772e6	-3.3416e8	4.3131e10

Table 2.2: The coefficient table of b_{mn}

m \ n	0	1	2	3	4
0	-8.7489e2	-1.4335e5	1.1955e8e7	-2.0911e10	9.5064e11
1	2.7551e1	9.4225e5	-4.1973e8	6.6190e10	-2.9289e12
2	9.6056e2	-1.2014e6	4.6413e8	-7.0841e10	3.0937e12
3	-5.9137e2	5.8176e5	-2.1273e8	3.2124e10	-1.3886e12
4	1.3101e2	-1.0342e5	3.6025e7	-5.3901e9	2.3005e11

The equations from [3] calculate the self-impedance of a strip dipole as:

$$R_{in}(\frac{l}{\lambda}, \frac{W}{\lambda}) = \sum_{m=0}^{5}\sum_{n=0}^{5} R_{mn}(\frac{l}{\lambda})^m(\frac{W}{\lambda})^n \tag{2.3}$$

$$X_{in}(\frac{l}{\lambda}, \frac{W}{\lambda}) = \sum_{m=0}^{5}\sum_{n=0}^{5} X_{mn}(\frac{l}{\lambda})^m(\frac{W}{\lambda})^n \tag{2.4}$$

The coefficients R_{mn} and X_{mn} can be found in Table 2.3 and Table 2.4.

Table 2.3: The coefficient table of R_{mn}

m \ n	0	1	2	3	4	5
0	211.4	-3.456e4	7.96e5	-5.796e6	2.535e7	2.089e8
1	-1486	5.072e5	-9.993e6	4.49e7	-2.478e8	0
2	-1.544e4	2.582e6	4.235e7	-5.274e7	0	0
3	2.047e5	4.834e6	-6.439e7	0	0	0
4	-7.511e5	-1.251e6	0	0	0	0
5	9.655e5	0	0	0	0	0

Table 2.4: The coefficient table of X_{mn}

m \ n	0	1	2	3	4	5
0	1022	-4.528e4	4.563e5	-2.015e6	4.277e6	-3.477
1	4.256e4	4.843e5	-6.868e6	2.478e7	-3.084e7	0
2	-4.147e6	2.13e7	-2.259e7	5.027e6	0	0
3	9.215e7	-3.885e8	2.088e8	0	0	0
4	-8.8e8	2.709e9	0	0	0	0
5	1.873e9	0	0	0	0	0

The resistance and reactance of the strip dipole antenna estimated by (2.3) and (2.4) are in Figure 2.2 and Figure 2.3.

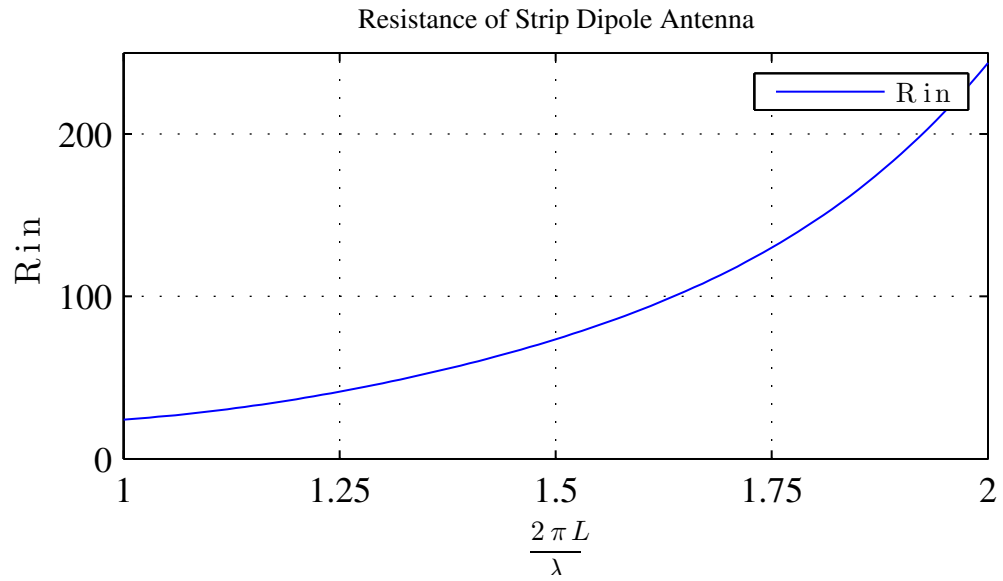

Figure 2.2: The resistance of strip dipole antenna

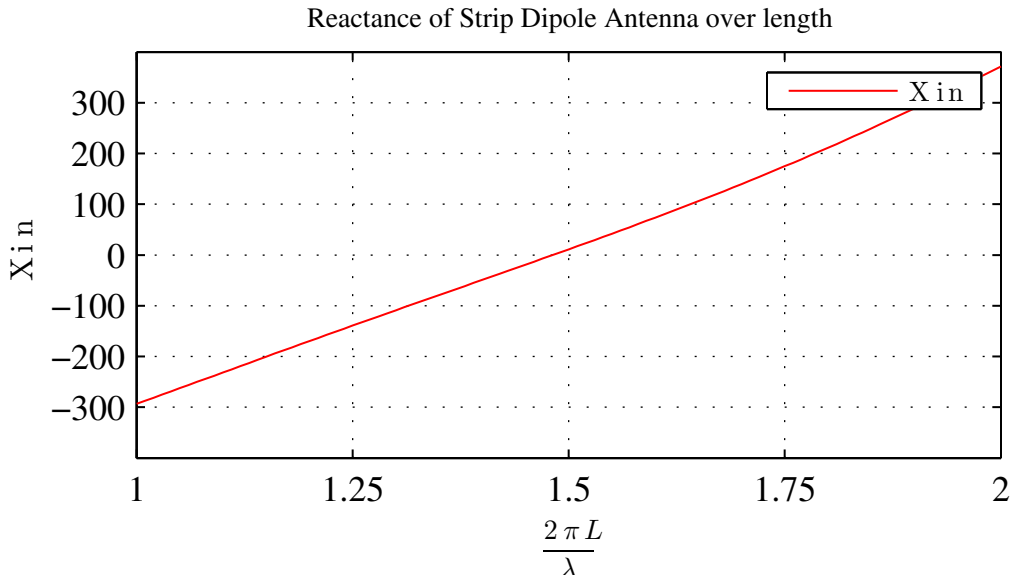

Figure 2.3: The reactance of strip dipole antenna

This method is verified to be practical in the range of $1.0 \leq kl \leq 2.0$ [4], and it shows that the strip dipole antenna has resonance ($X_{in} = 0$) when the electrical length is $kl \approx 1.5$, which represents half of the wavelength.

2.3 Cross Dipole Antenna

2.3.1 Cross Polarization

In electromagnetic theory, one important property which is defined by the orientation of the electric field (E) is called polarization. Two common polarizations are called linear polarization and circular polarization. In a linearly polarized system, the E vector is fixed along the direction of propagation, which means designers should be aware of the orientation of the antenna because the E vector is limited in one direction. Therefore, in many wireless communication applications, circular polarization is preferred where the trajectory of the tip of the E vector rotates about the propagation axis as a function of time. Circular polarization (CP) is widely used for satellite and ground station antennas, as circular polarization removes the need to continuously align the two apertures. A perfectly circularly polarized wave shown in Figure 2.4 and Figure 2.5 is generated by an antenna that simultaneously excites two orthogonal E vectors of equal amplitude and in phase quadrature [6].

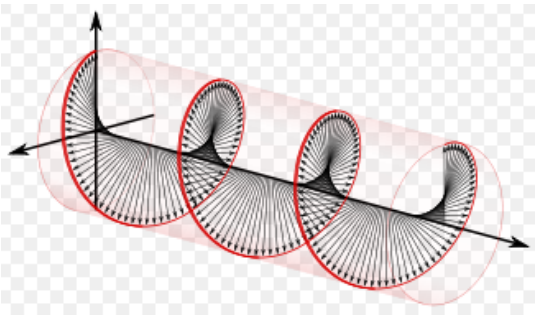

Figure 2.4: Right-hand circular polarization (reprinted with permission from Wikipedia)

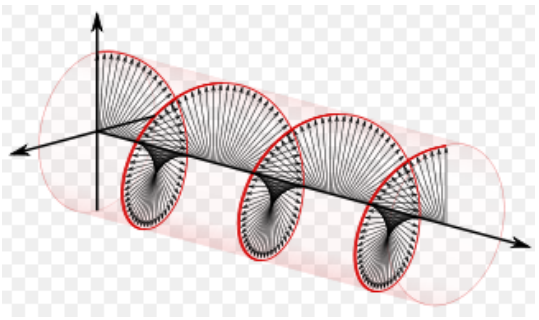

Figure 2.5: Left-hand circular polarization (reprinted with permission from Wikipedia)

From Figure 2.4 and Figure 2.5 we observe that the sense of a circularly polarized wave is determined by the rotation direction of the E vector. A right-hand cross polarization (RHCP) is generated when the rotation direction of the E field is clockwise, and for a left-hand cross polarization (LHCP), the electric field rotates counterclockwise [6]. Another important characteristic of cross polarization is called axis ratio (AR), which is defined as the ratio of the major to minor axes of the polarized wave. The spatial orientation is defined as the tilt angle (ψ in Figure 2.6) in the clockwise direction between a reference position and the major axis looking in the direction of propagation ($+z$ direction).

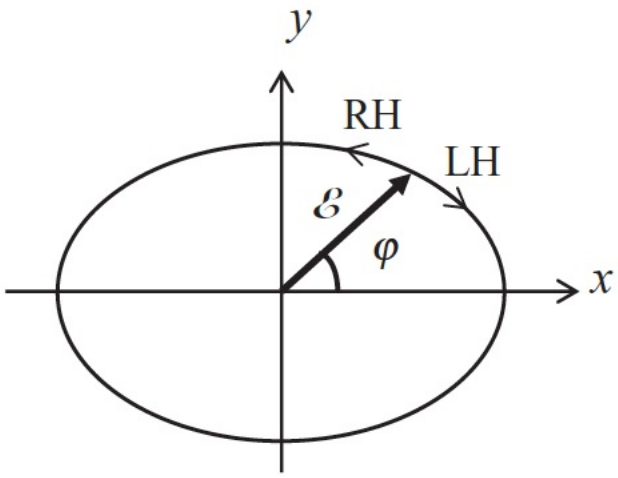

Figure 2.6: Polarization eclipse

If the complex voltage terms in the horizontal and vertical planes E_H and E_V have the same magnitude and in-phase quadrature ($\pm 90°$), these terms

may be combined to express either the LHCP or RHCP wave components.

$$E_{LHCP} = \frac{1}{\sqrt{2}}(E_H - jE_V) \tag{2.5a}$$

$$E_{RHCP} = \frac{1}{\sqrt{2}}(E_H + jE_V) \tag{2.5b}$$

Therefore, the radiation patterns that are generated by a CP antenna can be plotted by combining the amplitude and phase response of two orthogonal and linearly polarized waves.

2.3.2 Cross Dipole Antenna Mathematical Analysis

For linearly polarized radiating structure, the half-wavelength dipole antenna is widely used. It consists of two quarter-wavelength straight wire elements, which are fed in anti-phase by a voltage source located at the center. For obtaining circular polarization, a crossed dipole can be constructed by feeding two individual linear dipole antennas at 90 degrees. However, other than using two half-wavelength dipoles, the nominal length (i.e. $\lambda/2$) of two dipole antennas should be changed where the impedance of two elements at the center of two operating frequencies should be:

$$\text{Long element: } R1 + jX1\ \Omega$$

and

$$\text{Short element: } R2 + jX2\ \Omega$$

where the phase of the short element should be $\frac{\pi}{2}$ lag of long element. Moreover, for antennas operating in dual frequency mode, the long element should have resonance ($X_L \approx 0$) at lower frequency while the short element needs to have resonance at higher frequency. In order to obtain the desired dipole length, we examine the magnitude and phase of individual dipoles from the analytic equation over different lengths, and make pairs of two arbitrary lengths which have 90 degree phase difference. Table 2.5 shows the dipole length pair we found in the range $1.0 \leq kl \leq 2.0$.

Table 2.5: The impedance (cartesian and polar form) of dipoles of cross dipole antenna

Short(kl)	Rin	Xin	Magnitude	Phase	Long(kl)	Rin	Xin	Magnitude	Phase
1.18	33.56	-93.91	99.73	-70.33	1.53	86.11	30.11	91.22	19.27
1.19	34.49	-90.56	96.91	-69.15	1.54	88.50	33.96	94.79	20.99
1.20	35.44	-87.20	94.13	-68.14	1.55	90.96	37.83	98.51	22.58
1.21	36.42	-83.84	91.41	-66.52	1.56	93.49	41.72	102.37	24.05
1.22	37.42	-80.47	88.74	-65.06	1.57	96.09	45.62	106.38	25.40
1.23	38.44	-77.09	86.15	-63.50	1.58	98.78	49.56	110.51	26.64
1.24	39.49	-73.71	83.62	-61.82	1.59	101.55	53.50	114.78	27.78

2.4 Antenna Equivalent Circuit Model

Besides evaluating by analytical equation, the input impedance of antenna can also be easily demonstrated by an equivalent circuit model. Previously, Hamid and Hamid [7] developed an equivalent lumped-element circuit model for dipole antenna of arbitrary length. Therefore, following their circuit model, we can easily develop our own lumped-element model for the strip dipole we analyzed by mathematical equation. Moreover, after developing a circuit model for strip dipole antenna, we can also easily make a circuit model for the cross dipole circuit model by connecting two strip dipole antennas in parallel.

2.4.1 Circuit Model for Strip Dipole Antenna

According to Michael Hamid, a five-element RLC circuit model has already been developed to characterize the dipole antenna, which is shown in Figure 2.7.

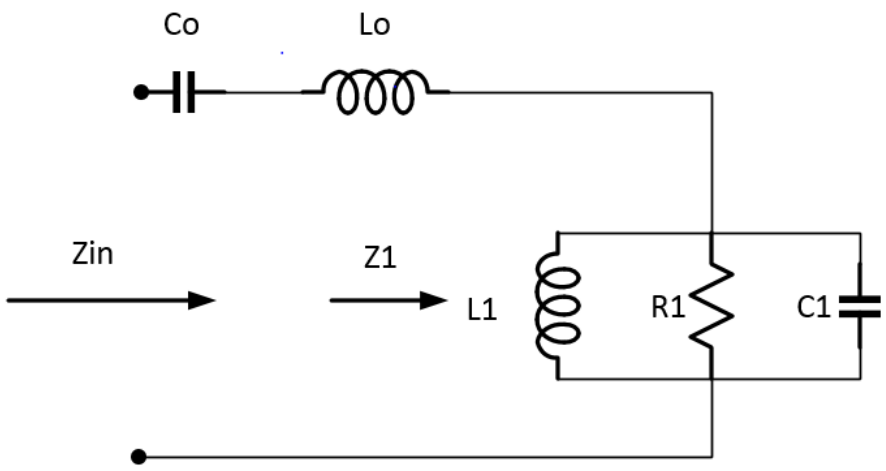

Figure 2.7: Antenna circuit model

This circuit is composed of a series LC circuit followed by a parallel RLC circuit. Because the input impedance function Z_{in} versus f can usually be represented as the ratio of two polynomials, where the zeros of the numerator are the zeros of the function and the zeros of the denominator are the poles of the function [7], each element in the circuit model can contribute to either pole or zero for the polynomial of antenna. Firstly, the impedance Z_{in} of the antenna usually contains a pole at f = 0, which can be modeled by a capacitor C_o, that has a reactance $-j/\omega C_o$. The value of C_o can be calculated by matching its reactance to antenna impedance under low-frequency range ($0 < 2h/\lambda < 0.25$). As frequency goes higher, however, C_o will play little role in antenna impedance and its reactance can be offset by a series inductor L_o. For the initial approximation, C_o is calculated from the antenna reactance at $2L/\lambda$, where $2L$ is the total length of the strip dipole. In this thesis, we computed the antenna reactance from the equations discussed in the previous section. The L_o is selected to resonate with C_0 at $2L/\lambda$, where the zero reactance happens.

After the effects of L_o and C_o have been extracted, the graph of the impedance function looks very similar to that of an RLC resonant network with a full-wave resonance at $2h/\lambda = 1$. For the circuit in Figure 2.6, we divided the circuit by two parts and labeled their impedances separately. We defined Z_o for the impedance of a series L_o, C_o circuit, and Z_1 for the

impedance of a parallel L_1, C_1, R_1 circuit. Since we have explained how to calculate L_o and C_o, we only need to calculate L_1, C_1 and R_1 based on Z_1. From the definition of the half-wavelength dipole antenna, we know that $X_{in} = 0$ when $2L/\lambda = 0.5$ and 1.0; therefore, we can determine the value of R1 to be the resistance when $X_{in} = 0$. Moreover, the values of L_1 and C_1 can also be calculated by setting $X_1 = 0$ at $2L/\lambda = 0.5$ and 1.0 because we already set $X_o = 0$ at these two locations.

Therefore, using the methods explained, we easily obtained the values listed in Table 2.6 for the five elements for a dipole antenna resonating at 420 MHz.

Table 2.6: Component values for antenna circuit model

C_o	1.05 pF
L_o	33 nH
C_1	0.5 pF
L_1	82.568 nH
$R1$	1170 Ω

The circuit simulations compared with the analytical equations for resistance and reactance are shown in Figure 2.8 and Figure 2.9.

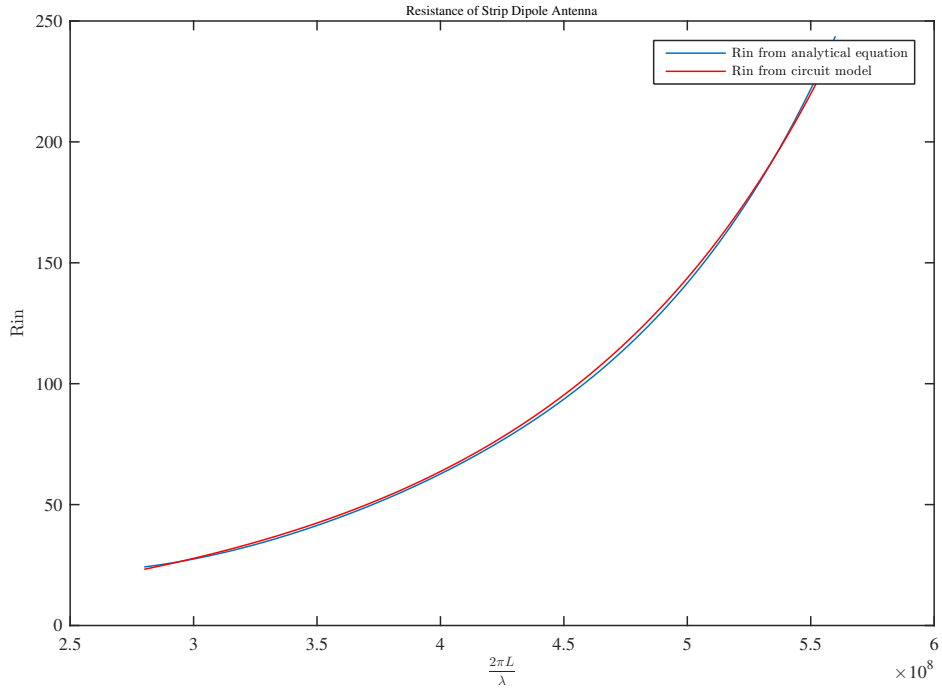

Figure 2.8: Circuit simulation and equation analysis of resistance

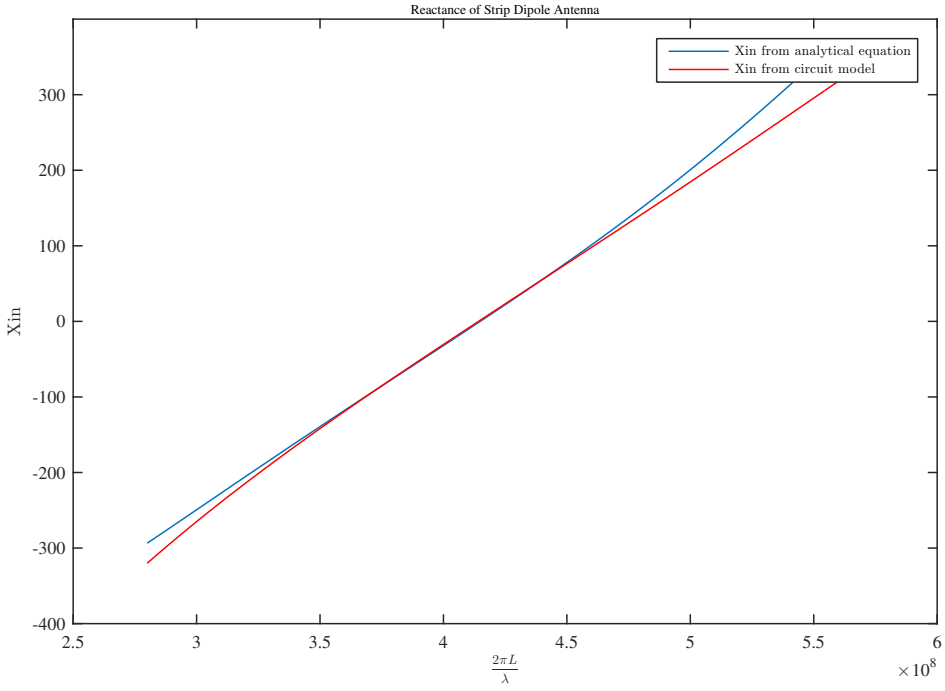

Figure 2.9: Circuit simulation and equation analysis of reactance

We can easily observe that the circuit model fits the analytical equations.

2.4.2 Circuit Model for Cross Dipole Antenna

The cross dipole antenna in this thesis, as explained in Section 2.4.1, is constructed by simply connecting two dipole antennas of different lengths in parallel. Therefore, the impedance for the cross dipole antenna can be calculated by paralleling two impedance functions of the two strip antennas. The circuit model for a cross dipole antenna is shown in Figure 2.10.

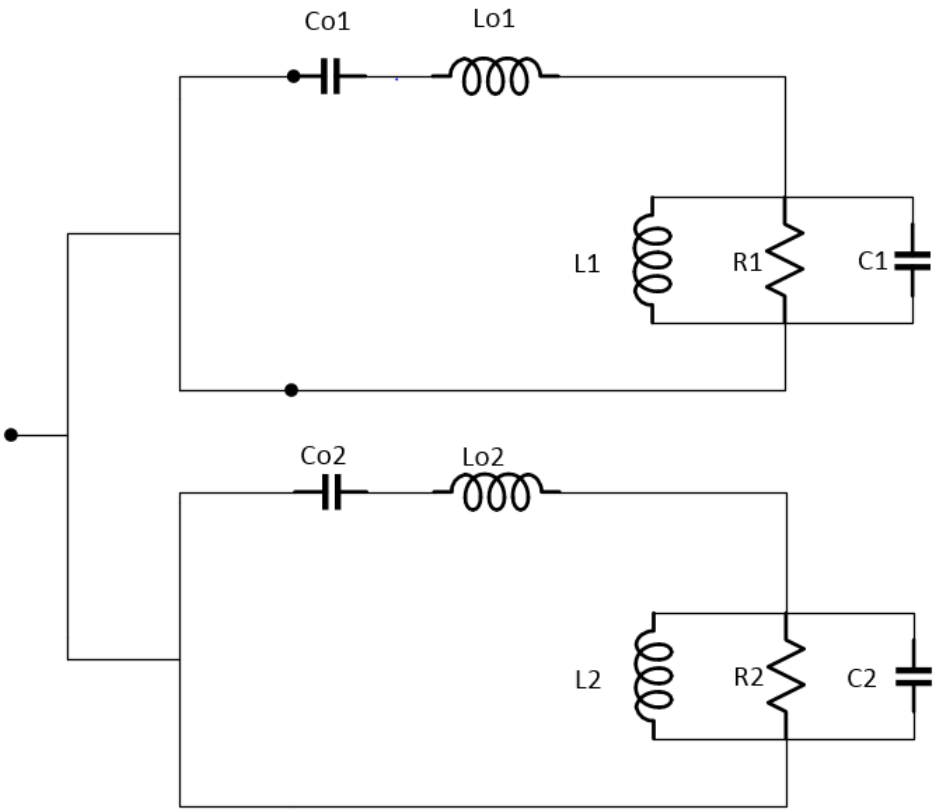

Figure 2.10: Circuit model for crossed dipole antenna

The value for each element is provided in Table 2.7.

Table 2.7: Component values of the cross dipole circuit model

C_{o1}	1.05 pF	C_{o2}	0.87 pF
L_{o1}	33 nH	L_{o2}	25nH
C_1	0.5 pF	C_2	0.22 pF
L_1	82.568 nH	L_2	133nH
R_1	1170 Ω	R_2	2700 Ω

The reflection coefficient of the cross dipole antenna from simulation is shown in Figure 2.11.

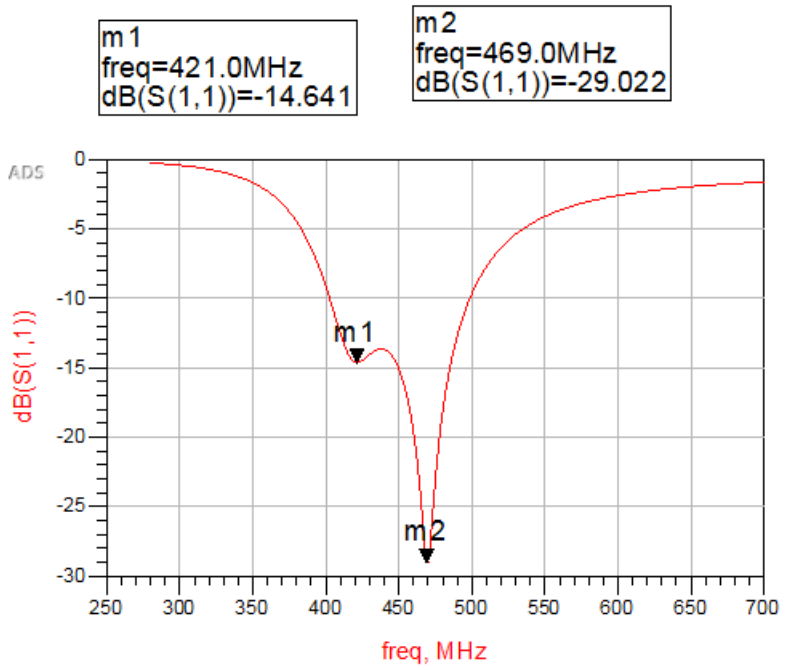

Figure 2.11: Reflection coefficient for cross dipole antenna

From the simulation of reflection coefficient, it is observed that the reflection coefficient has a local minimum at 420 MHz and 470 MHz, which means most of the signal power will be transferred from the antenna at these two frequencies. We also simulate the resistance and reactance of the cross dipole in Figure 2.12 and Figure 2.13.

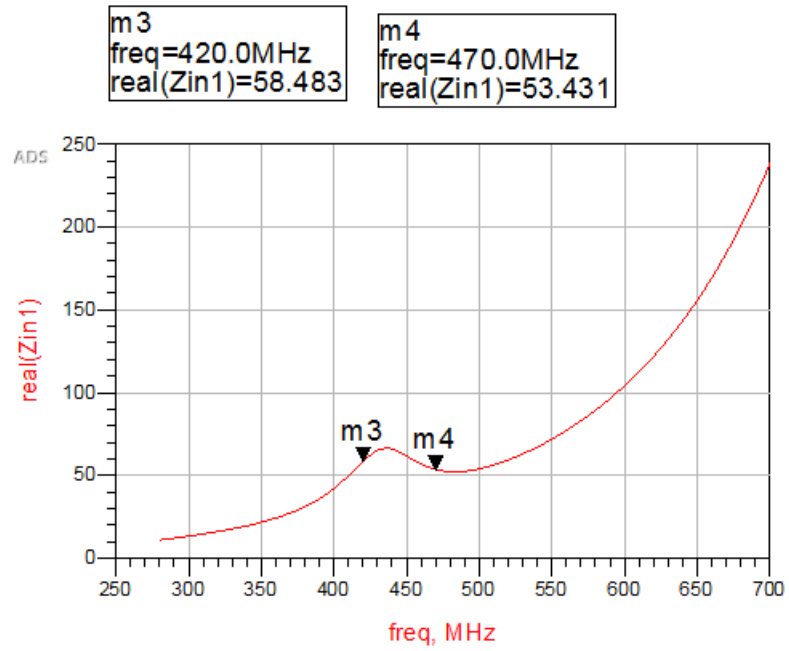

Figure 2.12: Resistance of cross dipole antenna

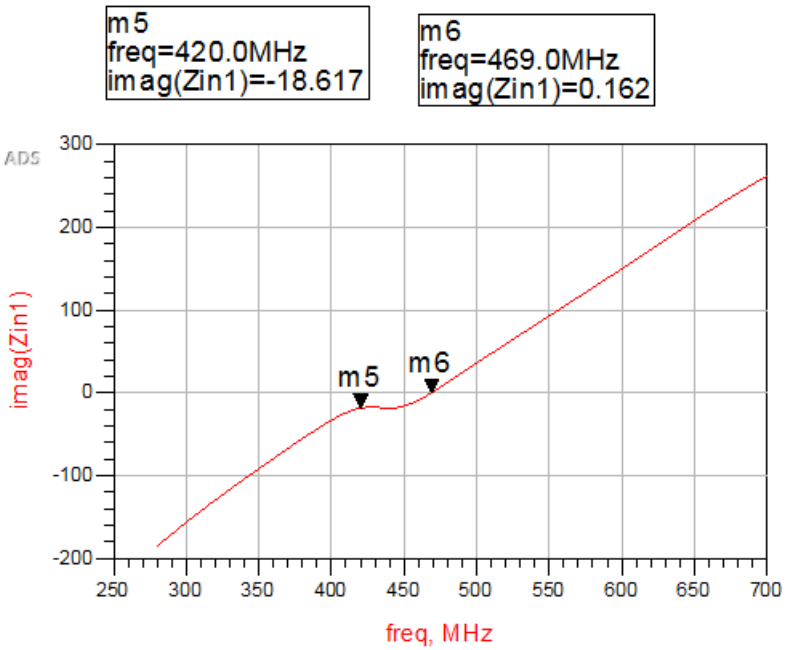

Figure 2.13: Reactance of cross dipole antenna

CHAPTER 3

DIPLEXER MODEL AND DESIGN

3.1 Introduction

The antenna we discussed in Chapter 2 is designed to operate in dual frequencies, and therefore we need to design a subsequent sub-system that separates the signal into two frequencies. Such a sub-system is called a diplexer. Typically, a diplexer is a three-port network that can split incoming signals from a common port (S) into two paths (or channels), which are usually called ports L and H [8]. The signals on ports L and H occupy disjoint frequency bands, and therefore, the signals on L and H coexist on port S without interfering with each other.

Usually, the signal on port L will cover a low frequency band while the signal on port H will occupy a higher frequency band. In such situations, a low-pass filter is used to connect ports L and S and a high-pass filter usually connects H and S. However, in many real applications, a band-pass filter is desired because microwave frequency bands are fully occupied by different applications (television, satellite, GPS, 3G, etc.). Therefore, two narrow band band-pass filters are commonly used in a diplexer structure. Figure 3.1 represents a simple block diagram of a diplexer.

3.2 Filter Basic

Generally, there are three kinds of filters—low-pass, high-pass and band-pass filters—distinguished by the frequency range of signals that can be passed through the filter. For the simplest diplexer design, a combination of low-pass and high-pass filters is usually used because a wide-band filter is easier to realize either with a transmission line or lumped element. However, in

modern wireless communication systems, the frequency spectrum is fully utilized by different applications. In this thesis, we are building a diplexer for a specific application, for instance, satellite communication, so we need to make sure the signals do not leak to other bands of the application, such as cellular communications. Therefore, the use of a band-pass filter is more desirable in our interface system. A common method of designing a band-pass filter will be discussed in the remainder of this chapter.

3.2.1 Filter Design by Insertion Loss Method

When designing a filter, we want the filter as close as possible to a perfect filter. A perfect filter means it has zero insertion loss in the passband [9], infinite attenuation in the stop band, and a linear phase response which can successfully avoid signal distortion in the passband. However, such an ideal filter is not practical, so we need to make our design based on tradeoffs, hence the art of filter design.

Among several filter design methods, the insertion loss method provides a systematic way to synthesize a filter response which maintains a reasonable control over the passband and stop band amplitude and phase characteristics. A filter designer can either choose a prototype for minimum insertion loss, or opt to design a filter with the shortest transition band, which means it should have the sharpest cutoff. Therefore, different prototypes of the filter can be chosen for different applications.

In the insertion loss method, a filter response is defined by insertion loss, P_{LR} [9]:

$$P_{LR} = \frac{Power\,available\,from\,source}{Power\,delivered\,to\,load} = \frac{P_{inc}}{P_{load}} = \frac{1}{1 - |\Gamma(\omega)|^2} \tag{3.1}$$

The insertion loss (IL) in dB is

$$IL = 10\,log P_{LR} \tag{3.2}$$

$\Gamma(\omega)$ is the reflection coefficient and depends on the operating frequency. It can be represented as

$$|\Gamma(\omega)|^2 = \frac{M(\omega^2)}{M(\omega^2) + N(\omega^2)} \tag{3.3}$$

where $M(\omega^2)$ and $N(\omega^2)$ are real polynomials in ω^2.

In this thesis, the minimum insertion loss at the passband is the parameter that we focus on most, and the sharpness of the filter is less important because for satellite application, a fair amount of isolation is enough. Therefore, a maximum flat prototype for the filter is chosen in this thesis.

3.2.2 Maximum Flat Filter Prototype

The characteristic of a maximum flat filter can also be called the binomial or Butterworth response. It provides the flattest passband response, but sacrifices the sharpness of the filter. For a low-pass filter, the insertion loss is represented as

$$P_{LR} = 1 + k^2(\frac{\omega}{\omega_c})^{2N} \tag{3.4}$$

where N is the order of the filter and w_c is the cutoff frequency. Therefore, we consider a second-order low filter, as shown in Figure 3.1.

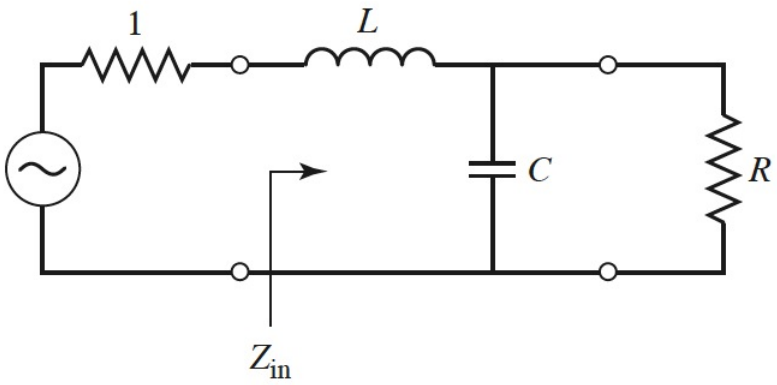

Figure 3.1: A second-order filter prototype

We can assume that the normalized impedance is 1 Ω, and the normalized

cutoff frequency is $w_c = 1$ rad/sec. The desired power ratio is

$$P_{LR} = 1 + w^4 \tag{3.5}$$

The input impedance of this filter is

$$Z_{in} = j\omega L + \frac{R(1 - j\omega RC)}{1 + \omega^2 R^2 C^2} \tag{3.6}$$

If we replace the reflection coefficient Γ with the input impedance Z_{in}, we can obtain the insertion loss as shown below, which is discussed in [9]:

$$P_{LR} = 1 + \frac{1}{4R}[(1 - R)^2 + (R^2C^2 + L^2 - 2LCR^2)\omega^2 + L^2C^2R^2\omega^4] \tag{3.7}$$

Compared with the desired insertion loss we obtained previously, we should get $P_{LR} = 1$ for $\omega = 0$ for $R = 1$. Therefore,

$$C^2 + L^2 - 2LC = (C - L)^2 = 0 \tag{3.8}$$

The coefficient of ω^4 should be 1; then

$$L = C = \sqrt{2} \tag{3.9}$$

Therefore, we can apply this procedure to a filter with an arbitrary number of order (but not a large number). A low-pass filter prototype beginning with a series element is chosen in this thesis.

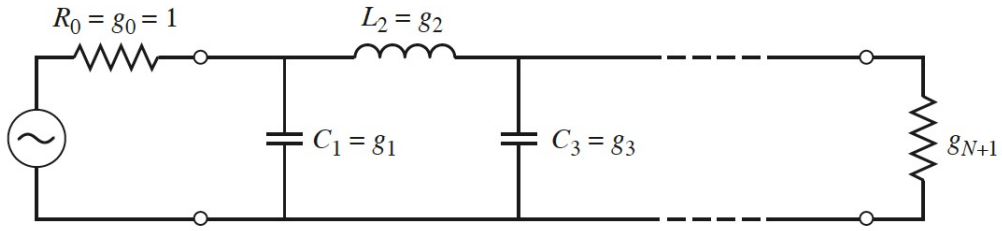

Figure 3.2: Low-pass filter prototype beginning with a series element

In Figure 3.2, the element values of the filter are numbered from g_0 to g_{N+1}; g_{N+1} represents the load resistance, while all other numbers in the middle are the values for the reactive elements. From Figure 3.2 we can observe that these reactive elements are arranged alternatively in the parallel and series

connections. Table 3.1 represents a table for elements in the maximum flat filter prototype.

Table 3.1: Element values for maximally flat low-pass filter prototype

N	g_1	g_2	g_3	g_4	g_5	g_6	g_7	g_8	g_9	g_{10}	g_{11}
1	2.0000	1.0000									
2	1.4142	1.4142	1.0000								
3	1.0000	2.0000	1.0000	1.0000							
4	0.7654	1.8478	1.8478	0.7654	1.0000						
5	0.6180	1.6180	2.0000	1.6180	0.6180	1.0000					
6	0.5176	1.4142	1.9318	1.9318	1.4142	0.5176	1.0000				
7	0.4450	1.2470	1.8019	2.0000	1.8019	1.2470	0.4450	1.0000			
8	0.3902	1.1111	1.6629	1.9615	1.9615	1.6629	1.1111	0.3902	1.0000		
9	0.3473	1.0000	1.5321	1.8794	2.0000	1.8794	1.5321	1.0000	0.3473	1.0000	
10	0.3129	0.9080	1.4142	1.7820	1.9754	1.9754	1.7820	1.4142	0.9080	0.3129	1.0000

We can easily design a low-pass filter based on the prototype and element values given in Table 3.1, which will be discussed in Section 3.2.3.

3.2.3 Low-Pass Filter Design

The maximally flat low-pass filter prototype discussed in Section 3.2.2 is based on source impedance of $R_s = 1\,\Omega$ and a cutoff frequency of $\omega_c = 1$ rad/sec. Such design can be scaled by impedance and frequency, and transformed to high-pass, band-pass or band-stop filters. Impedance scaling means scaling the element values by source and load impedance while frequency scaling means converting the element values according the change in the cutoff frequency ω_c. For impedance scaling, if the source and load impedance are R_0, the new filter component values are given by

$$L' = R_0 L \tag{3.10a}$$

$$C' = \frac{C}{R_0} \tag{3.10b}$$

$$R_s{}' = R_0 \tag{3.10c}$$

$$R'_L = R_0 R_L \tag{3.10d}$$

where L, C, and R_L are the component values for the original prototype. The frequency scaling changes a low-pass filter prototype's cutoff frequency

from unity to ω_c by scaling the frequency dependence of the filter by the factor $1/\omega_c$, and it can be obtained by replacing ω by ω/ω_c. Therefore, the insertion loss now becomes:

$$P_{LR}^{'}(\omega) = P_{LR}(\frac{\omega}{\omega_c}) \tag{3.11}$$

where now ω_c is the new cutoff frequency and cutoff occurs when $\omega/\omega_c = 1$. Now the new element values can be obtained by applying substitution of ω with $\frac{\omega}{\omega_c}$ into the series reactance and the shunt susceptance:

$$jX_k = j\frac{\omega}{\omega_c}L_k = j\omega L_k^{'} \tag{3.12a}$$

$$jB_k = j\frac{\omega}{\omega_c}C_k = j\omega C_k^{'} \tag{3.12b}$$

Therefore the new element values are:

$$L_k^{'} = \frac{L_k}{\omega_c} \tag{3.13a}$$

$$C_k^{'} = \frac{C_k}{\omega_c} \tag{3.13b}$$

When both impedance scaling and frequency scaling are required, we combined both (3.10) and (3.13). Therefore, the new element values can be represented as:

$$L_k^{'} = \frac{R_0 L_k}{\omega_c} \tag{3.14a}$$

$$C_k^{'} = \frac{C_k}{R_0\omega_c} \tag{3.14b}$$

Therefore, the lumped element values of a low-pass filter can be obtained by the above equations based on a cutoff frequency and the original values of the prototyped filter. In Section 3.2.4, we will study the design of a band-pass filter.

3.2.4 Band-Pass Filter Design

We already know that any low-pass filter can be designed based on the procedure in Section 3.2.3 when given the cutoff frequency ω_0 and filter prototype. In this subsection the design procedure of the band-pass filter will be dis-

cussed. The low-pass filter prototype can also be transferred to band-pass or band-stop application. Suppose we want to design a band-pass filter with center frequency ω_0, and ω_1 and ω_2 denote the pass-band edges (frequency at which the loss is 3 dB larger than the loss at center frequency); then the following frequency substitution can be made:

$$\omega \leftarrow \frac{\omega_0}{\omega_2 - \omega_1}(\frac{\omega}{\omega_0} - \frac{\omega_0}{\omega}) = \frac{1}{\Delta}(\frac{\omega}{\omega_0} - \frac{\omega_0}{\omega}) \tag{3.15}$$

where

$$\Delta = \frac{\omega_2 - \omega_1}{\omega_0} \tag{3.16}$$

represents the fractional bandwidth of the filter. Therefore, the transformation in (3.15) can be mapped into the low-pass filter prototype, as we did in the last subsection. Then the relation will be:

$$\frac{1}{\Delta}(\frac{\omega}{\omega_0} - \frac{\omega_0}{\omega}) = 0, when\, \omega = \omega_0 \tag{3.17a}$$

$$\frac{1}{\Delta}(\frac{\omega}{\omega_0} - \frac{\omega_0}{\omega}) = -1, when\, \omega = \omega_1 \tag{3.17b}$$

$$\frac{1}{\Delta}(\frac{\omega}{\omega_0} - \frac{\omega_0}{\omega}) = 1, when\, \omega = \omega_2 \tag{3.17c}$$

Then we can use Equation (3.15) to find the expressions for the series reactance and shunt susceptance. The series reactance can be represented as:

$$jX_k = \frac{j}{\Delta}(\frac{\omega}{\omega_0} - \frac{\omega_0}{\omega})L_k = j\frac{\omega L_k}{\Delta\omega_0} - j\frac{\omega_0 L_k}{\Delta\omega} = j\omega L_k^{'} - j\frac{1}{\omega C_k^{'}} \tag{3.18}$$

Therefore, the series LC circuit has element values

$$L_k^{'} = \frac{L_k}{\Delta\omega_0} \tag{3.19a}$$

$$C_k^{'} = \frac{\Delta}{\omega_0 L_k} \tag{3.19b}$$

where L_k and C_k are element values after impedance scaling.

Similarly, the shunt susceptance should be

$$jB_k = \frac{j}{\Delta}(\frac{\omega}{\omega_0} - \frac{\omega_0}{\omega})C_k = j\frac{\omega C_k}{\Delta\omega_0} - j\frac{\omega_0 C_k}{\Delta\omega} = j\omega C_k^{'} - j\frac{1}{\omega L_k^{'}} \tag{3.20}$$

Therefore, the element values in the shunt LC circuit are

$$L_k^{'} = \frac{\Delta}{\omega_0 C_k} \tag{3.21a}$$

$$C_k^{'} = \frac{C_k}{\Delta\omega_0} \tag{3.21b}$$

Finally, with the design procedure presented in this subsection, we can easily design a band-pass filter in the maximally flat prototype.

3.2.5 Band-pass Filter Design Example

Suppose we want to design a third-order maximally flat type band-pass filter in a 50 Ω system, with the center frequency set to 420 MHz and 3dB bandwidth set to 10%. Only lumped element can be used for the filter. Therefore, the procedure discussed in the previous subsection can be followed. First, because a third-order filter is desired, the element values for the filter will be:

$$g_1 = 1.000 \tag{3.22a}$$

$$g_2 = 2.000 \tag{3.22b}$$

$$g_3 = 1.000 \tag{3.22c}$$

The new component level after impedance scaling will be:

$$L_1 = R_0 g_1 = 50 \tag{3.23a}$$

$$C_2 = \frac{g_2}{R_0} = \frac{1}{100} \tag{3.23b}$$

$$L_3 = R_0 g_3 = 50 \tag{3.23c}$$

We started the design with a series LC circuit, so the filter circuit will be a series LC circuit cascade with shunt LC circuit and cascade again with a series LC circuit. Therefore, the series LC circuits have element values:

$$L'_{1,3} = \frac{L_{1,3}}{\Delta\omega_0} = 189.47\ \text{nH} \tag{3.24a}$$

$$C'_{1,3} = \frac{\Delta}{\omega_0 L_{1,3}} = 0.7579\ \text{pF} \tag{3.24b}$$

Similarly, the shunt LC circuit has element values:

$$L'_2 = \frac{\Delta}{\omega_0 C_k} = 3.789\ \text{nH} \tag{3.25a}$$

$$C'_2 = \frac{C_k}{\Delta\omega_0} = 37.89\ \text{pF} \tag{3.25b}$$

After calculating the values for the lumped elements, we constructed a simple filter in our simulator, Advanced Design Systems (ADS). The circuit schematic in the simulator is shown in Figure 3.3.

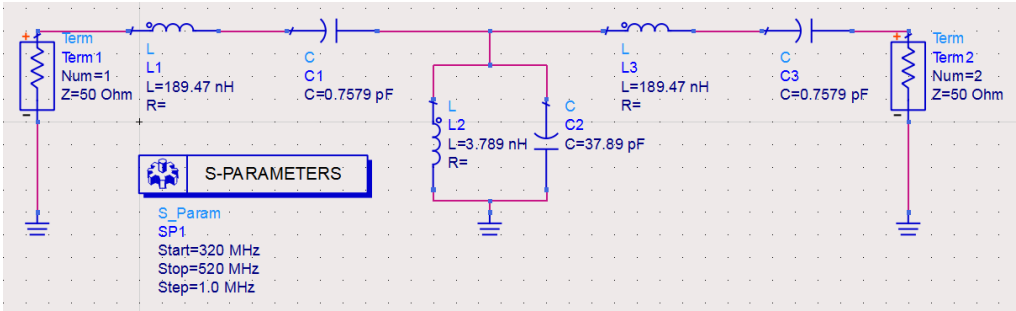

Figure 3.3: Schematic of the sample filter

The simulation of the filter is shown in Figure 3.4.

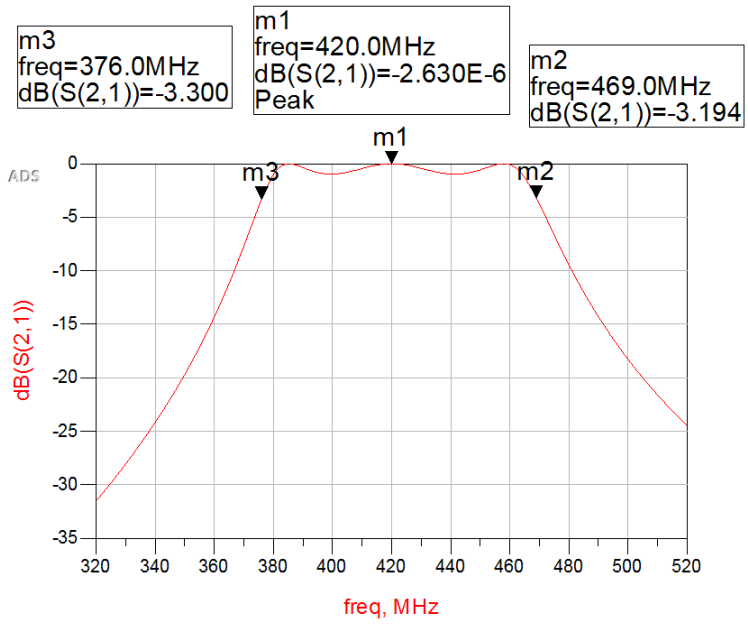

Figure 3.4: Simulation of the sample filter

From the simulation result, we can observe that the filter response has a peak at the desired frequency, 420 MHz, and its 3 dB bandwidth at each side are 12% and 13% respectively. Therefore, the procedure is valuable for calculating the filter parameters.

3.2.6 Band-pass Filter Using Capacitively Coupled Shunt Resonator

A band-pass filter using a capacitively coupled shunt resonator, as shown in Figure 3.5, is a type of filter where short-circuited shunt resonators are capacitively coupled with series capacitors [6]. Moreover, for Nth-order filters, N short-circuited stubs will be used, and they are usually slightly less than $\frac{\lambda}{4}$. The equations for calculating the parameters are listed below and the details can also be found in [6]. Firstly, we derive the admittance constant [6]:

$$Z_0 J_{01} = \sqrt{\frac{\pi\Delta}{4g_1}} \tag{3.26a}$$

$$Z_0 J_{n,n+1} = \frac{\pi\Delta}{4\sqrt{g_n g_{n+1}}} \tag{3.26b}$$

$$Z_0 J_{N,N+1} = \sqrt{\frac{\pi\Delta}{4 g_N g_{N+1}}} \tag{3.26c}$$

Similarly, the coupling capacitor values can be found as

$$C_{01} = \frac{J_{01}}{\omega_0 \sqrt{1 - (Z_0 J_{01})^2}} \tag{3.27a}$$

$$C_{n,n+1} = \frac{J_{n,n+1}}{\omega_0} \tag{3.27b}$$

$$C_{N,N+1} = \frac{J_{N,N+1}}{\omega_0 \sqrt{1 - (Z_0 J_{N,N+1})^2}} \tag{3.27c}$$

Next, we need to calculate the length of the stub. Firstly we need ΔC_n, which represents the change in capacitance caused by the parallel addition of the inverter elements.

$$\Delta C_n = -C_{n-1,n} - C_{n,n+1} \tag{3.28}$$

Then the overall stub length is given by

$$l_n = \frac{\lambda}{4} + \left(\frac{Z_0 \omega_0 \Delta C_n}{2\pi} \right) \lambda \tag{3.29}$$

The equations above are sufficient for the calculation band-pass filter using capacitively coupled shunt resonators.

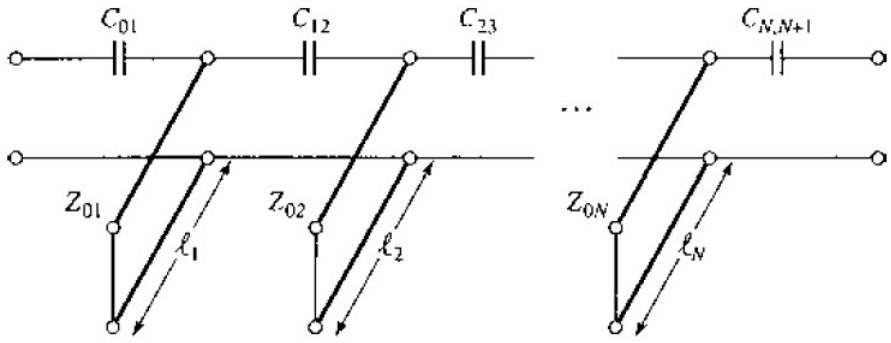

Figure 3.5: A band-pass filter using capacitively coupled shunt stub resonators

3.2.7 Filter Performance with Various Order and Bandwidth

Another issue that is important for diplexer design is filter performance under different filter orders and different bandwidths. Because the increase of filter order can help increase the sharpness of the filter, but will also increase the insertion loss as the tradeoff, it is necessary for us to analyze the sensitivity of filter performance (i.e. insertion loss and rejection) versus filter order and bandwidth. The sensitivity analysis was performed by measuring the insertion loss (S(2,1)) at 420 MHz (desired frequency) and at 470 MHz (undesired frequency), with only lumped elements being used and Q_C at 100, Q_L at 50. The results are included in Table 3.2 and Table 3.3.

Table 3.2: S(2,1) at 420 MHz for band-pass filter centered at 420 MHz

FBW \ N	1	2	3	4	5	6	7
5 %	-3.216	-5.26	-7.542	-9.984	-12.278	-14.669	-17.078
8 %	-2.142	-3.369	-4.798	-6.309	-7.776	-9.299	-10.812
10 %	-1.753	-2.71	-3.858	-5.042	-6.249	-7.459	-8.678
13 %	-1.377	-2.095	-2.978	-3.911	-4.817	-5.758	-6.693
15 %	-1.208	-1.821	-2.577	-3.371	-4.178	-4.991	-5.807
18 %	-1.019	-1.52	-2.155	-2.825	-3.485	-4.158	-4.841

Table 3.3: S(2,1) at 470 MHz for band-pass filter centered at 420 MHz

FBW \ N	1	2	3	4	5	6	7
5 %	-13.45	-26.49	-39.83	-53.05	-66.13	-79.42	-92.96
8 %	-9.581	-18.61	-27.75	-37.02	-46.02	-55.62	-64.57
10 %	-8.222	-14.93	-22.213	-29.685	-37.264	-43.94	-51.69
13 %	-6.417	-10.85	-16.097	-21.213	-25.803	-31.51	-36.87
15 %	-5.598	-8.95	-12.518	-16.388	-20.625	-24.38	-28.41
18 %	-4.61	-6.51	-8.685	-11.231	-13.672	-15.92	-18.64

From Table 3.2 and Table 3.3, it can be concluded that as the order of the filter increases, the insertion losses at both desired frequency (420 MHz) and undesired frequency (470 MHz) increase. Moreover, as the bandwidth of

filter increases, the filter will gain less insertion loss at both desired frequency and undesired frequency. Therefore, since we need a very low insertion loss at the desired frequency, a third-order filter with 13 % bandwidth is chosen.

3.3 Diplexer Design

In the previous section, the basic of filter has been thoroughly discussed. In this section, several diplexer designs (combination of two band-pass filters) will be discussed. These designs include designs with only microstrip lines, designs with only lumped elements, and designs with both kinds of elements. Each design has its own advantage and disadvantage and a final design will be selected in Chapter 5.

3.3.1 Design Using Stub Tuner

Figure 3.6 is a diplexer design using the stub tuner, functioning to split signals in 420 MHz and signals in 470 MHz.

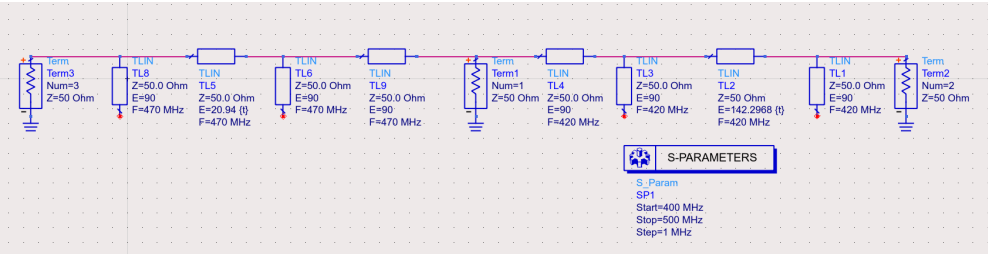

Figure 3.6: Diplexer with stub tuner

The general idea of this design is to block each frequency at each arm. For a quarter wavelength transmission line ($E = 90^o$) with an open load ($Z = \infty$), the input impedance is zero because quarter wavelength transmission transmits from open to short. Therefore, a quarter wave open stub at a particular frequency is usually used to block signal at that frequency. Moreover, the lengths of "TL5" and"TL2" were determined by the tuning optimization, which is a feature in our simulator, ADS.

The simulation result of this diplexer is shown in Figure 3.7.

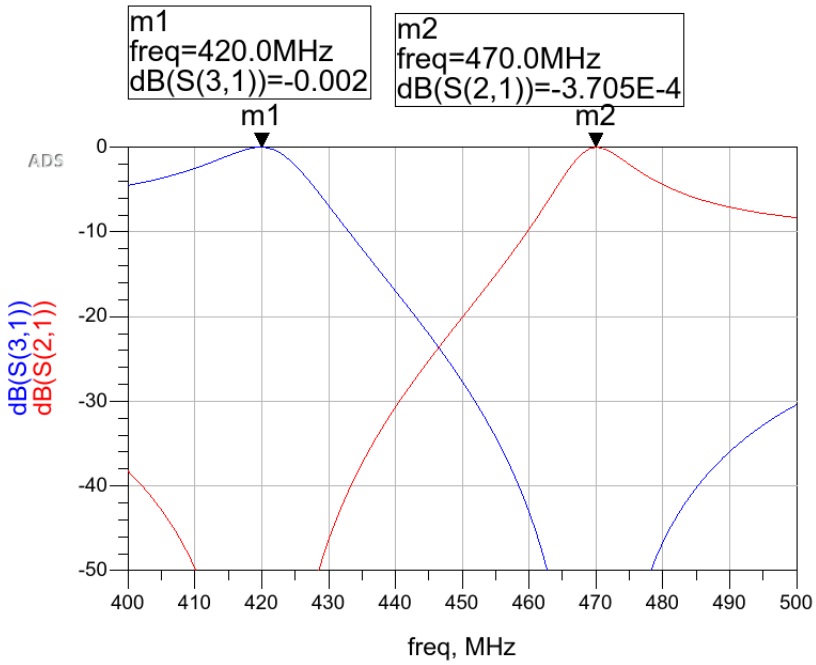

Figure 3.7: Diplexer with stub tuner simulation

From the simulation above we observe that the diplexer has almost no insertion loss at two desired frequencies (because all elements used are ideal). What is more, the crosstalk is over 50 dB, which indicates it is a good diplexer design. However, if we calculate the size of this diplexer and we assume wavelength $\lambda = 40$ cm, we find the length is 58 cm and width is 10 cm, which shows that the diplexer size is very large. Therefore, we need to try a better design.

3.3.2 Design Using Lumped Element

The general idea of designing a diplexer with a lumped element is to design two band-pass filters first and then combine them together. Therefore, there are several prototypes of the band-pass filter such as Butterworth, equal-ripple and maximum delay. In our diplexer design we choose the equal-ripple band-pass filter because it has the least flatness when filters are compared in the same order [5]. We choose the filter with the most sharpness because we want transducer gain (S21) as high as possible at the desired frequency while we want it as low as possible at the undesired frequency. The way to design band-pass filters has already been discussed in the previous section.

In our design, we choose a third-order 0.5 dB ripple band-pass filter; the design circuit is shown in Figure 3.8.

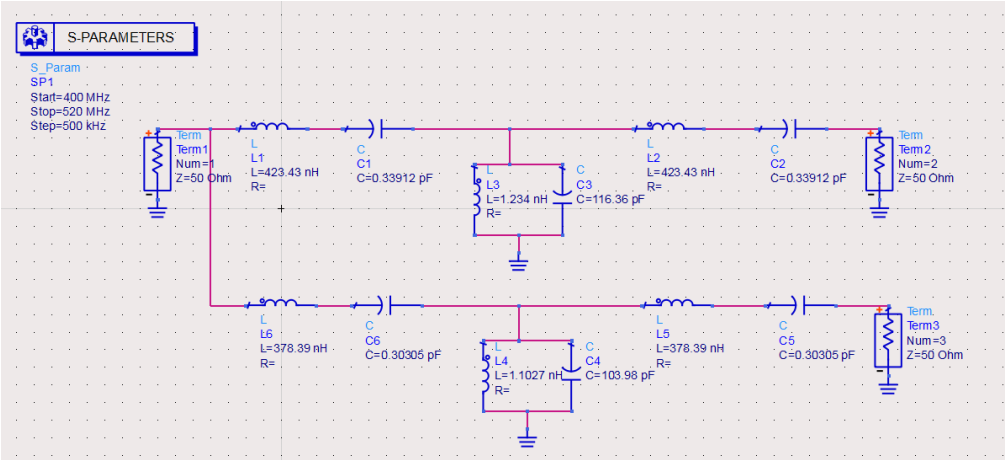

Figure 3.8: Diplexer with lumped element

The simulation of this diplexer design is in Figure 3.9.

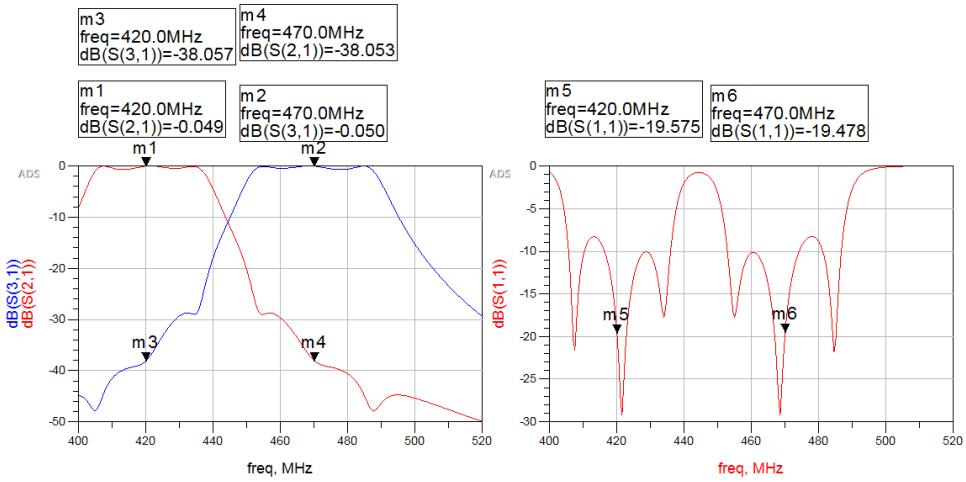

Figure 3.9: Diplexer with lumped element simulation

From the simulation result above we can observe that the diplexer has about 0.05 dB insertion loss at the desired frequency and the diplexer has crosstalk of 38 dB, which indicates good isolation. However, when we checked the reflection coefficient (S11), we found it was higher than expected because we did not add the matching network. After we added a matching network, the diplexer is shown in Figure 3.10.

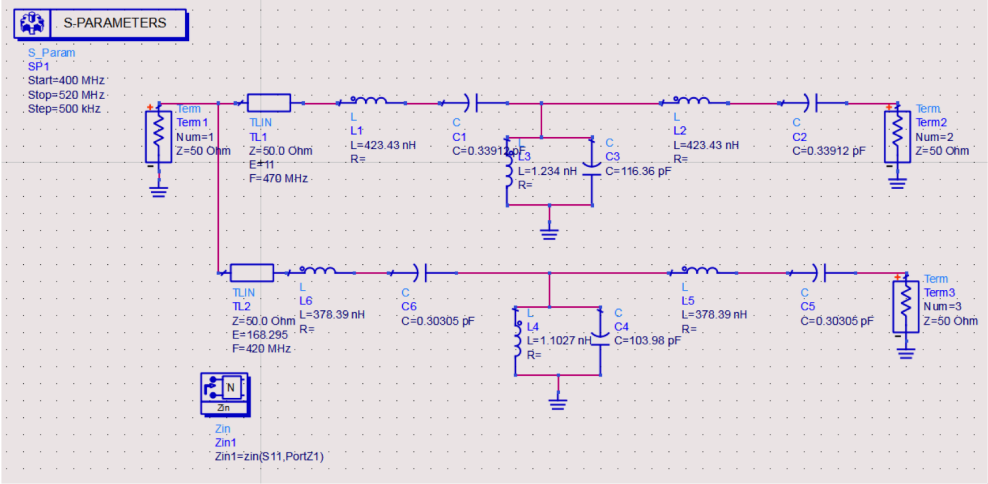

Figure 3.10: Diplexer with lumped element with matching network

The simulation result of the diplexer with a matching network now becomes one shown in Figure 3.11. Now it is easy to see that diplexer has higher reflection.

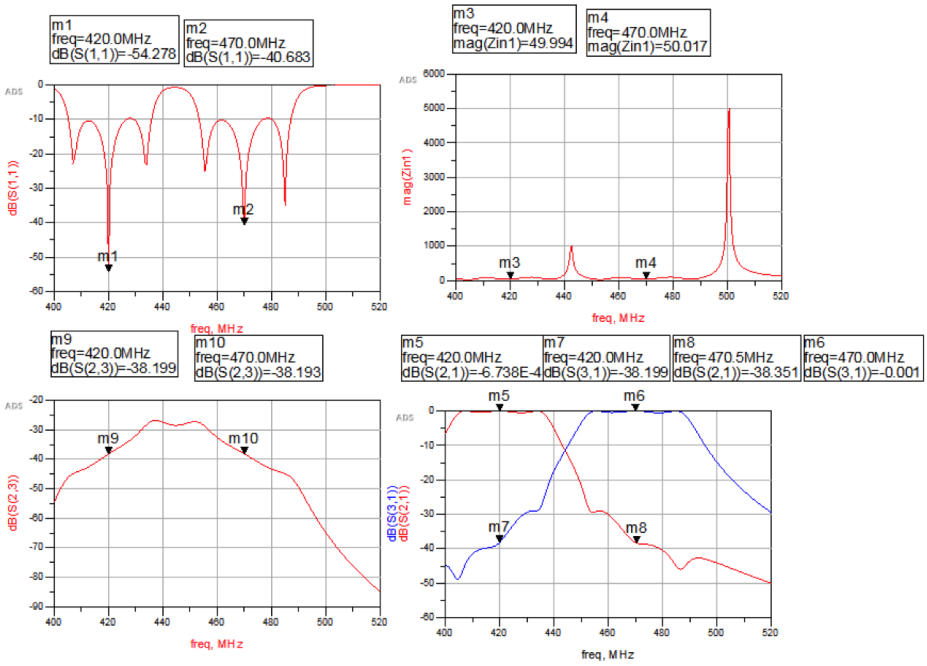

Figure 3.11: Simulation of diplexer with lumped element with matching network

However, although now we can solve the board size issue, another problem arises. As we can see in the schematic, the value of some capacitors is as small

as 0.3 pF, which is usually readily controllable in a PCB board. Therefore, we need to consider a hybrid design.

3.3.3 Hybrid Design

In order to compensate for the limitations of both lumped and distributed elements, we develop a hybrid design including both lumped elements and distributed elements. This design is called a capacitively coupled shunt resonator band-pass filter, which is discussed in the previous section. The schematic is shown in Figure 3.12 and the simulation result is in Figure 3.13.

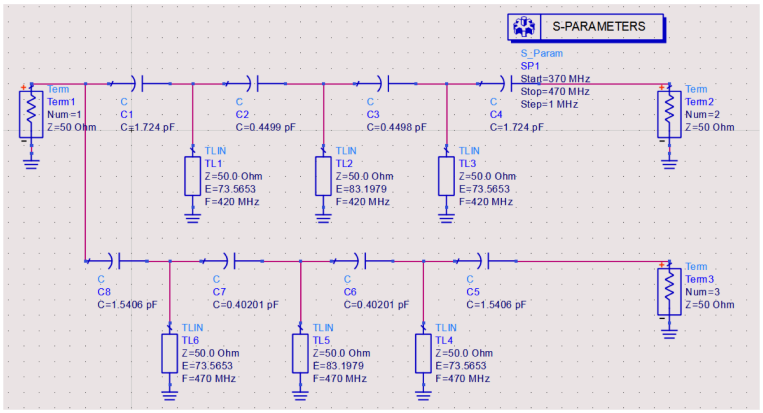

Figure 3.12: Diplexer designed by coupled capacitively shunt resonator stub

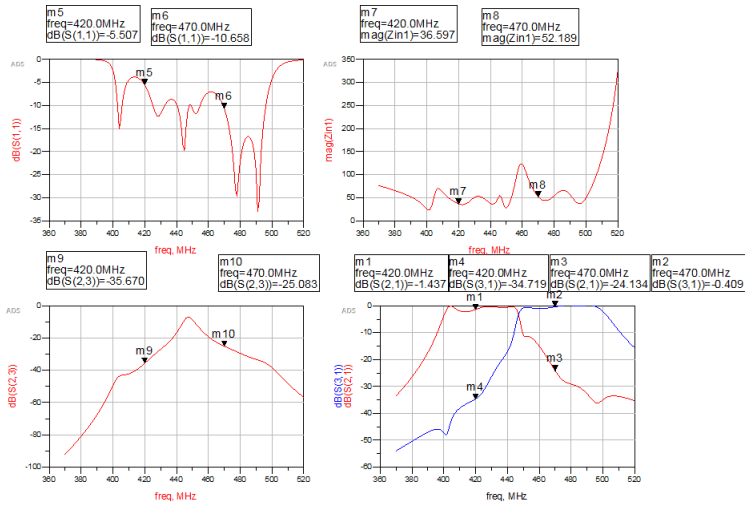

Figure 3.13: Simulation of diplexer by coupled capacitively shunt resonator

The hybrid design has overcome the limitation of area and lumped element values in the previous two designs, and it also shows great performance as a dual-frequency filter. However, the filter will suffer from the sensitivity of the lumped element to the parasitics from the PCB board. For instance, for the diplexer shown in Figure 3.13, if the PCB board adds 0.2 pF to each capacitor, the performance of the diplexer, which is shown in Figure 3.14, varies a lot.

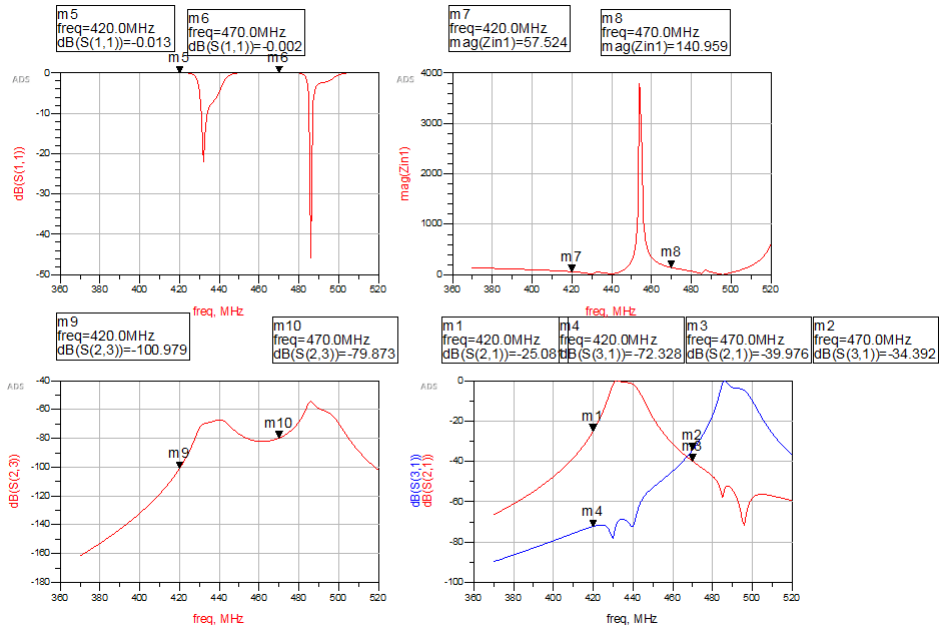

Figure 3.14: Sensitivity influence on diplexer

CHAPTER 4

COMBINATION OF ANTENNA AND DIPLEXER

4.1 Introduction

In Chapters 2 and 3, we discuss the characterization of the antenna and the design of the diplexer separately. We have successfully characterized the cross dipole antenna and designed the diplexer under a 50 Ω system. In this chapter, we will discuss how can we effectively combine the antenna and diplexer together, i.e. how to transfer maximum power from the antenna to the diplexer. The method we used to accomplish it is to build an impedance matching network. If an ideal matching network is used, the impedances seen from both sides of any terminal port of the circuit should be equal. We will start by explaining the theory of the impedance matching network, and then discuss the topology we used for matching the network.

4.2 Matching Network Basics

Impedance matching is always an essential part of the design process for a microwave component or system [9]. The basic idea of impedance matching, as shown in Figure 4.1, is to place a matching network between the source impedance and load impedance. Ideally, the matching network is lossless, to avoid unnecessary loss of power, and is always designed so that when looking into the matching network, the impedance seen is Z_0, which is the characteristic impedance of the system. Therefore, with the ideal matching network, no reflections will be received at the source, which means all the power should be transferred to the load impedance.

As long as the load impedance, Z_L, has a positive real part, a matching network can always be found. There are many types of matching networks

available as choices; however, factors also exist to determine the best choice of matching networks. The matching network includes the following [9]:

- *Complexity* − We always prefer simpler designs for most engineering solutions. Matching networks with simpler structures can be cheaper, smaller, more reliable, and less lossy than more complex designs.
- *Bandwidth* − Any type of matching network can perform the perfect match at a single frequency. In many applications, however, it is essential to match a load impedance over a band of frequencies.
- *Implementation* − Depending on the type of materials being used, one type of matching network may be preferable to another.
- *Adjustability* − In some applications the matching network may require adjustment to match a variable load impedance.

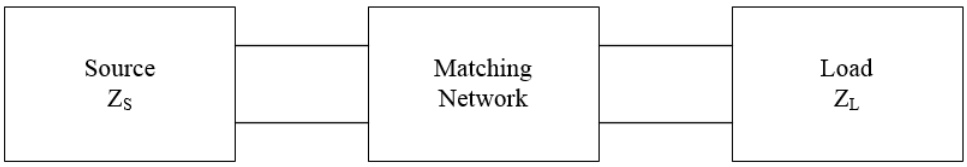

Figure 4.1: A matching network between source and load impedance

4.2.1 Matching with Lumped Elements (L Network)

Since the reactance of the dipole will approach zero at the two frequencies, the impedance matching between source and load impedance can be considered as matching between two resistances. For resistive terminations, the easiest way to match them is using an L-network, which means the impedance matching network only contains inductors and capacitors. Figure 4.2 and Figure 4.3 show us how we can make a impedance matching network between two resistances [10]:

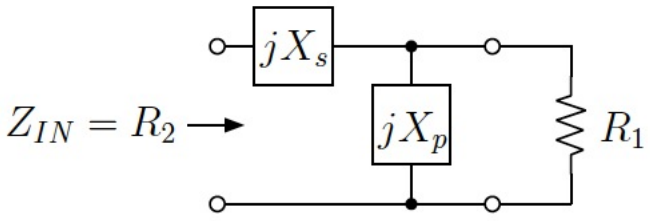

Figure 4.2: L-network for impedance matching

The parallel reactance X_p can be transformed to series reactance as shown in Figure 4.3 [6].

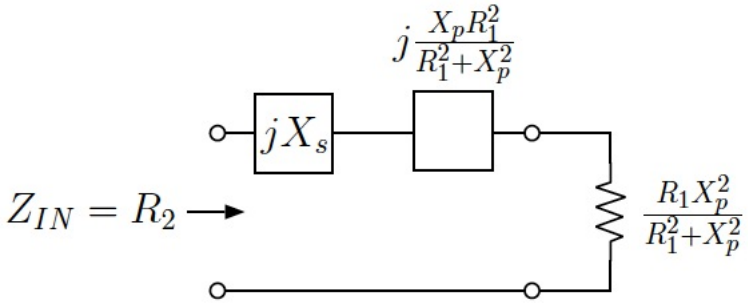

Figure 4.3: Parallel-to-series transformation

If we want the input impedance equal to R2, then we use the following equations.

$$X_s = -\frac{X_pR_1^2}{R_1^2 + X_p^2} \tag{4.1a}$$

$$R_2 = \frac{R_1X_p^2}{R_1^2 + X_p^2} \tag{4.1b}$$

Solving the equations above gives us:

$$X_p = \pm R_1\sqrt{\frac{R_2}{R_1 - R_2}} \tag{4.2a}$$

$$X_s = \mp\sqrt{R_2R_1 - R_2^2} \tag{4.2b}$$

Note that there are two possible solutions which therefore yield two different

circuit solutions. The solutions are referred to as "low-pass" and "high-pass" respectively, and are illustrated in Figure 4.4 and Figure 4.5.

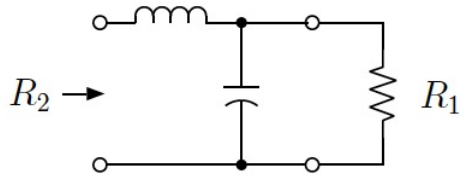

Figure 4.4: Low-pass L-network

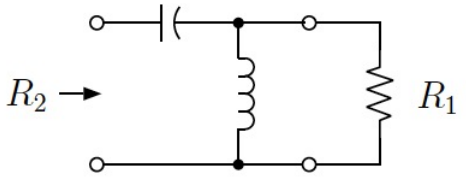

Figure 4.5: High-pass L-network

4.3 Matching Network Design between Diplexer and Cross Dipole Antenna

From the circuit simulation of the cross dipole antenna in Section 2.4, we observed that the cross-dipole demonstrated close resistance (53 Ω and 58 Ω) and also showed low reactance ($-j18$ Ω and $-j0.62$ Ω) at two operating frequencies (i.e. 420 MHz and 470 MHz). Therefore, based on the approach discussed in Section 4.2, we can build a matching network between 50 Ω and 58 Ω, and we obtained two solutions for our matching network circuit, which are shown in Figure 4.6 and Figure 4.7.

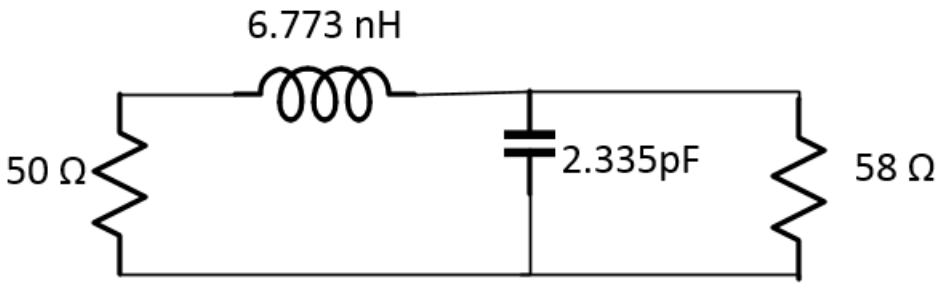

Figure 4.6: Low-pass matching network

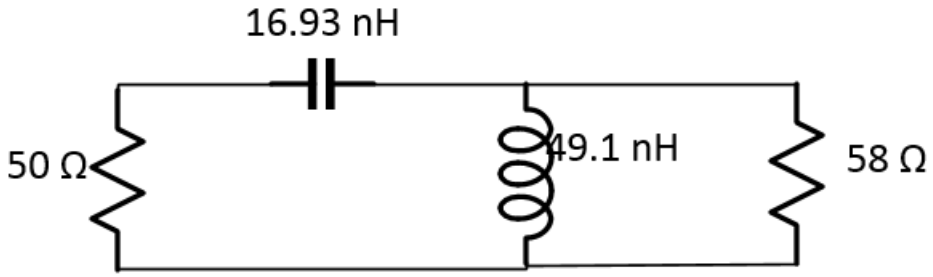

Figure 4.7: High-pass matching network

Since for this thesis, we only took a first step into the matching network design, we did not perform the full implementation task on both the antenna and the diplexer. However, if we consider that the system impedance from the diplexer is 50 Ω, we can still get an initial idea of the validity of the matching network.

CHAPTER 5

IMPLEMENTATION AND FABRICATION

5.1 Introduction

In the previous chapters, the designs for antennas and diplexers have been discussed. In this chapter, the final design and implementation of the diplexer will be discussed. The diplexer was constructed on a PCB board and its performance was measured with a vector analyzer. For the final design, we chose the capacitively coupled shunt resonator as the filter topology because it saves PCB board area. The measurement phase for the whole front-end was divided into three parts: measurement of single filter, measurement of diplexer, and measurement of diplexer combined with the antenna. Finally, after the measurement, the result was compared with the simulated result, and further optimization work was performed to meet requirements. Although, due to the time limitation, the whole implementation of both antenna and diplexers has not been accomplished, it is believed to be accomplishable since the implementation of the diplexer has proved successful.

5.2 Microstrip Transmission Line Characterization

Before we start the implementation, it is necessary to characterize the microstrip transmission. A Microstrip line is one of the most popular types of planar transmission line primarily because it can be fabricated by photolithographic processes and is easily miniaturized and integrated with both passive and active microwave devices. The geometry of a microstrip line is shown in Figure 5.1. A conductor of width W is printed on a thin, grounded dielectric substrate of thickness d and relative permittivity ϵ_r; the sketch of the field lines is shown in Figure 5.2.

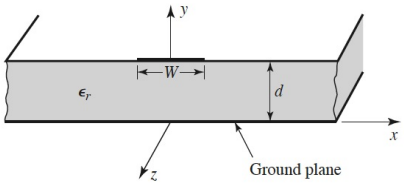

Figure 5.1: Microstrip transmission line geometry

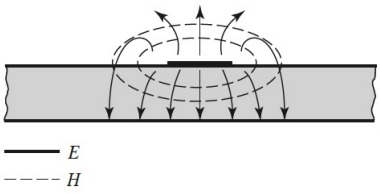

Figure 5.2: Electric and magnetic field lines

Theoretically, microstrip lines can be considered to support quasi-TEM mode propagation. In fact, many successful microstrip designs and evaluations utilize TEM-mode results from transmission line theory. Therefore, it is helpful to review TEM-mode RF transmission line theory. Readers may find the review of TEM-mode transmission lines in Appendix A useful.

For this section in the thesis, we fabricated a couple of microstrip lines to verify their characterization (i.e. phase velocity v_p and effective dielectric constant ϵ_e). The fabricated microstrip lines are shown in Figure 5.3.

Figure 5.3: Layout for microstrip characterization

The longer line is 1.85 inches and the shorter line is 1.3 inches. We characterized the lines by measuring the phase of their reflection (S11) at different frequencies, extracting their phase velocity, calculating the effective dielectric constant and verifying it with theoretical calculation.

The phase of reflection coefficient for the longer microstrip line is shown in Table 5.1 and the phase of reflection coefficient for the shorter microstrip line is shown in Table 5.2.

Table 5.1: Phase of Reflection for Longer Microstrip Line

Frequency (MHz)	Phase (deg)
100	-14.64
200	-28.91
300	-42.86
400	-56.70
500	-70.33
600	-83.88
700	-97.37

Table 5.2: Phase of Reflection for Shorter Microstrip Line

Frequency (MHz)	Phase (deg)
100	-7.91
200	-15.70
300	-23.40
400	-31.08
500	-38.69
600	-46.40
700	-54.18

We then calculated the differences of phases at every 100 MHz, averaged the differences, and obtained the phase velocity. The calculation procedure is:

$$v_p = \lambda * f = Length\, of\, microstrip * \frac{360}{averaged\, difference\, /2} \tag{5.1}$$

The phase difference is divided by 2 because during the measurement the signal travels roundtrip, from microstrip lines to the measurement unit (VNA) and back to microstrip lines. The phase velocity for the longer microstrip line is $1.64e8$ m/s and the phase velocity for shorter microstrip line is $1.65e8$ m/s.

After extracting the phase velocity, we need to verify if we can get a valid effective dielectric constant, ϵ_e. The theoretical value for effective dielectric constant, according to [7], is:

$$\epsilon_e = \frac{\epsilon_r + 1}{2} + \frac{\epsilon_r - 1}{2} \frac{1}{\sqrt{1 + 12d/W}} \tag{5.2}$$

where ϵ_r is relative dielectric constant, d is the thickness of substrate, and W is the width of conductor. In our implementation, we are using a 1-ounce FR4-copper board [8], whose dielectric constant ϵ_r is 4.4, width W is 115 mil and thickness d is 60 mil. Therefore, the calculated value for effective dielectric constant is 3.33. Afterward, we calculated the effective dielectric

constant by using the phase velocity, which can be represented as:

$$\epsilon_e = \left(\frac{c}{v_p}\right) \tag{5.3}$$

Therefore, the effective dielectric constants for the longer and shorter microstrip lines are 3.346 and 3.305, respectively, which are approximately the same as the theoretical values. Thus, the characterization of the microstrip line has been verified to be consistent with the theoretical value.

5.3 Filter Implementation

For the topology of the band-pass filters, the capacitively coupled shunt resonators are chosen because of space savings compared with traditional band-pass filters (i.e. cavity resonators) operating in these frequencies. The construction of the filter was accomplished through a printed circuit board, and its basic layout is shown in Figure 5.7. FR-4 was chosen for substrate material and copper was used as the conductor. The width of conductors is 0.115 mil to make the characteristic impedance of the microstrip transmission line to be 50 Ω. Since we do not have very accurate capacitors at this moment, we make appropriate ones by connecting the capacitors we already have.

5.3.1 First-order Filter Implementation

We began our implementation of filters with the simplest structure, a capacitively-coupled shunt resonator based first-order band-pass filter. The first-order band-pass filter, as shown in Figure 3.5, contains one microstrip stub in the center and one capacitor on each side. However, because the stub in the center is very long at our operating frequency range, $\frac{1}{8}$ wavelength of the stub is replaced by inductors based on Richard transformation [9], where the transformation is shown in Figure 5.4.

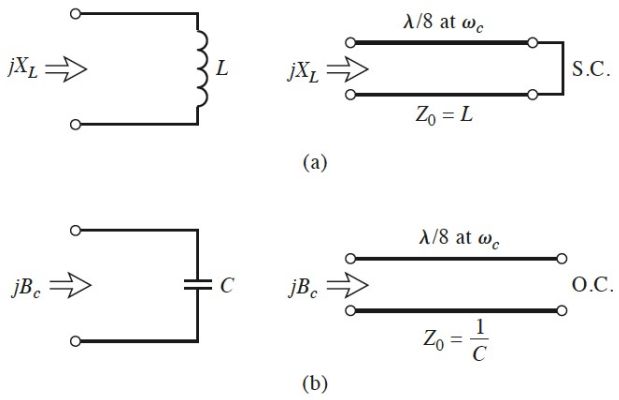

Figure 5.4: Richards' transformation for (a) an inductor to a short-circuited stub, and (b) a capacitor to an open-circuited stub

The reactance of an inductor can be written as:

$$jX_L = j\Omega L = jL\tan\beta l \tag{5.4}$$

which indicates that an inductor can be replaced with a short-circuited stub of length βl and characteristic impedance L. Therefore, an inductor value can be obtained using the equation above at the desired frequency. The final design that contains capacitors, inductors, and microstrip stubs is shown Figure 5.5. Its simulation performance in the ADS is in Figure 5.6.

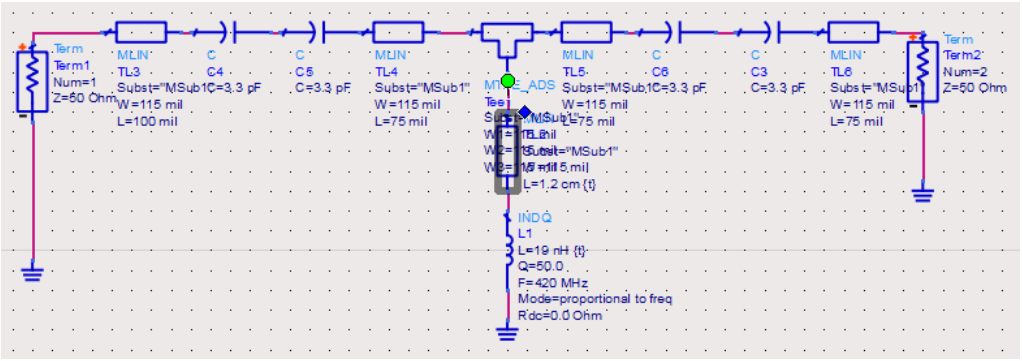

Figure 5.5: First-order filter implementation

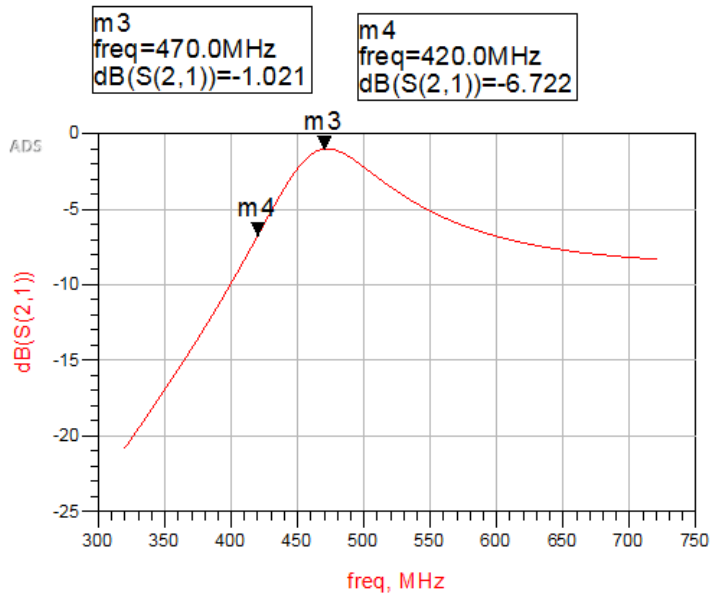

Figure 5.6: First-order filter implementation simulation

After validating the performance of the first-order band-pass filter, the actual filter was fabricated in the PCB board. The board is shown in Figure 5.7.

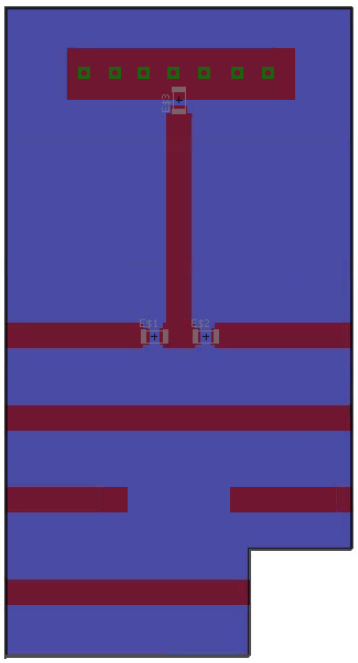

Figure 5.7: First-order filter layout

We measured the performance of the band-pass filter using the vector network analyzer, and we calibrated the PCB board first before we made the measurement. Readers can find the concept of calibration in Appendix B. The measurement of the first-order bandpass filter is shown in Figure 5.8.

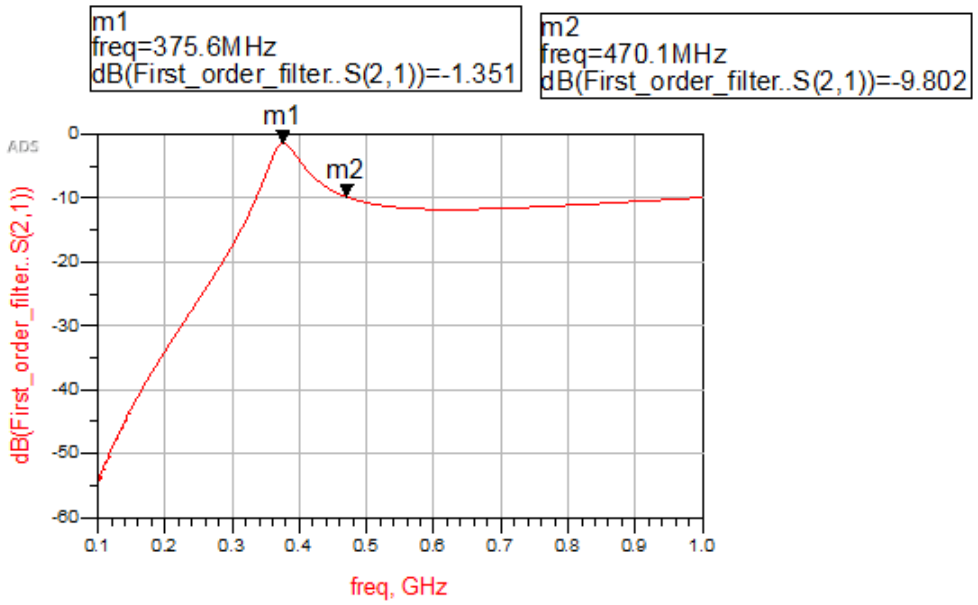

Figure 5.8: First-order filter measurement

As we can see from the result above, the S21 does not reach maximum at the desired frequency, 420 MHz. Therefore, the inductor value was tuned in order to compensate for the influence from coupling capacitors and inductor leads. The result of the tuned filter is shown in Figure 5.9.

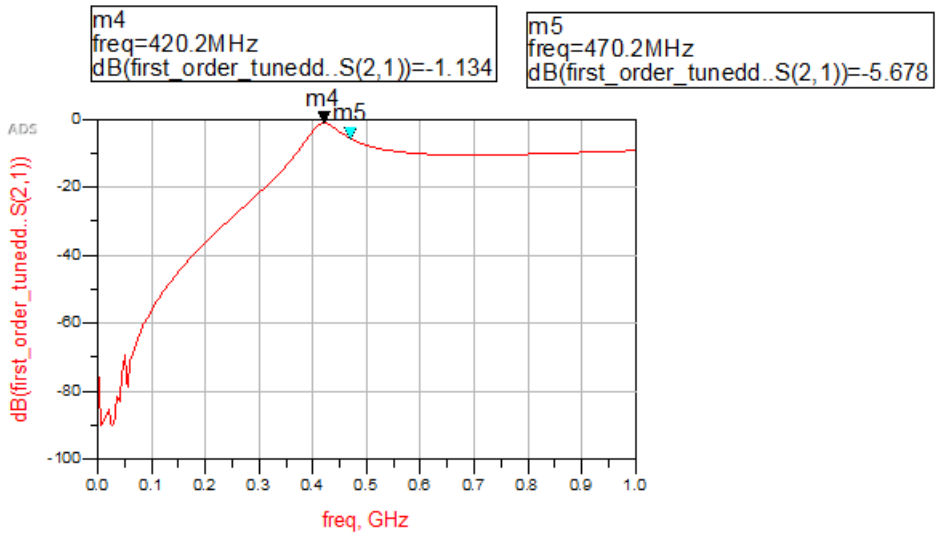

Figure 5.9: First-order filter measurement after tuning

As we can see from the results, the filter has an insertion loss of 1.134 dB, and the insertion loss at 470 MHz (another operating frequency in dual-mode) is 5.678 dB.

5.3.2 First-Order Diplexer Implementation

After the successful implementation of the first-order filter, we stepped to the implementation of the first-order diplexer. We combined two first-order filters operating in two frequencies by setting them up in parallel. The schematic of the designed diplexer is shown Figure 5.10, and the simulation performance of the diplexer is shown in Figure 5.11.

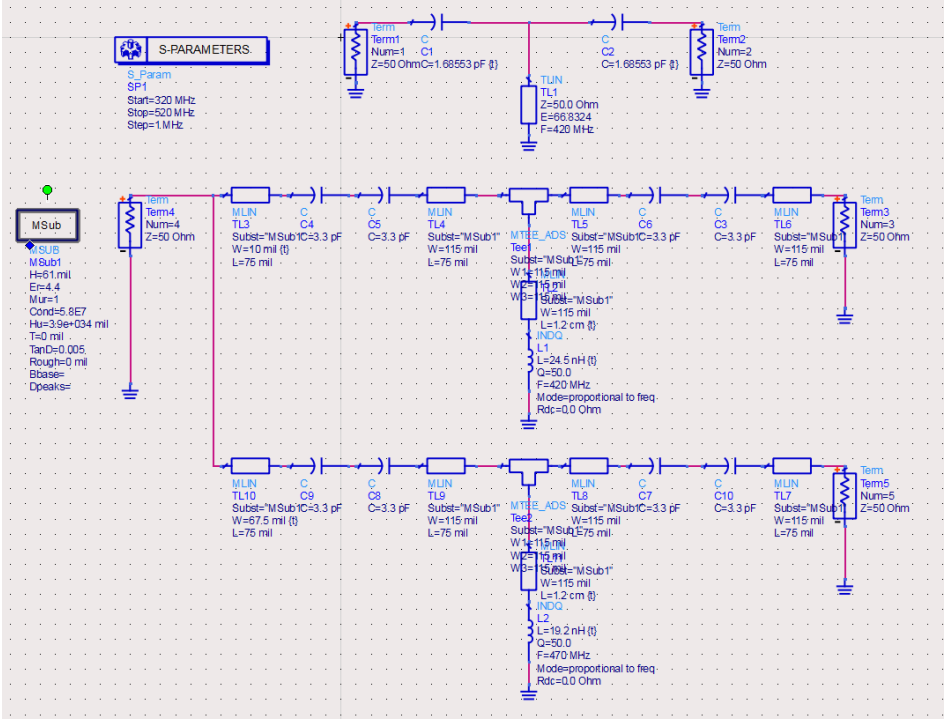

Figure 5.10: First-order diplexer schematic

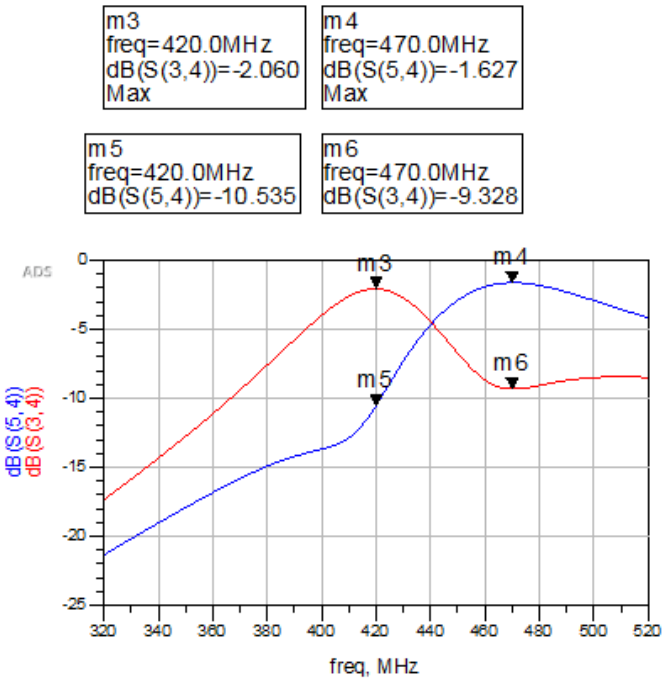

Figure 5.11: First-order diplexer simulation

From the simulation result, we can observe that the filter branch working at 420 MHz has an insertion loss of 2 dB, while demonstrating an insertion loss of 10 dB. The filter operating at 470 MHz also shows similar performance in desired and undesired frequencies. The result is reasonable because although the first-order filter does not show too much isolation, the diplexer still shows some levels of separation for the filter in these two frequencies.

With the simulation result, we also constructed a first-order diplexer on the PCB with microstrip line and lumped elements. The layout for our diplexer is shown in Figure 5.12.

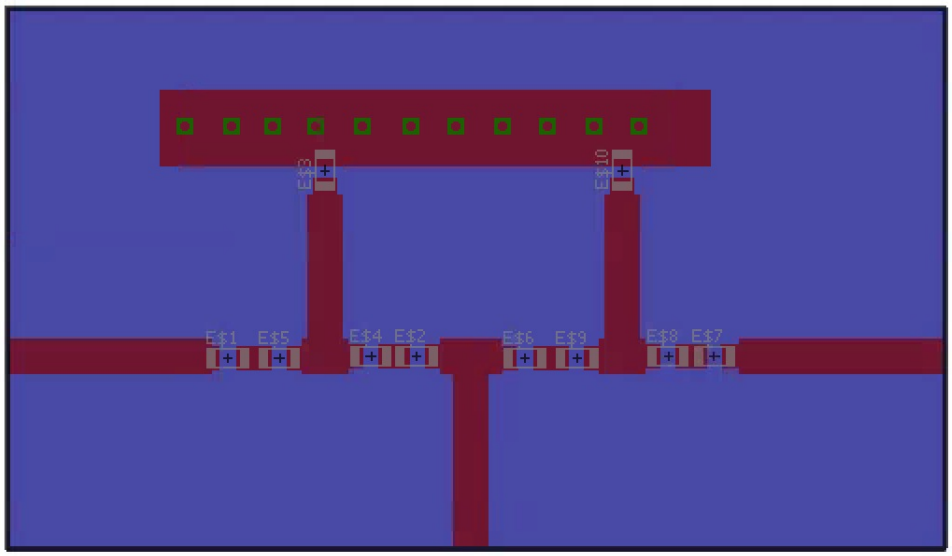

Figure 5.12: Layout for first-order diplexer

However, for this diplexer, we did not set its working frequency the same as we did in the simulator. We just randomly picked two close operating frequencies and tried to demonstrate the performance of the diplexer in the PCB. The measurement for our diplexer is shown in Figure 5.13.

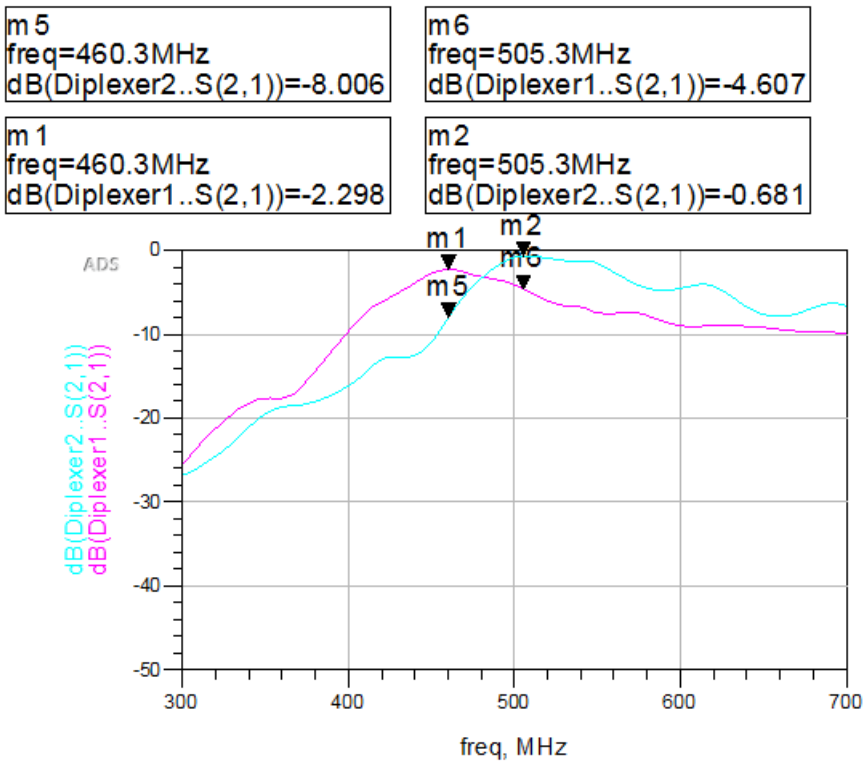

Figure 5.13: Measurement of first-order diplexer

From the measurement result, we observe that the diplexer can show two different filter performances. Each filter has low insertion loss at its operating frequency and higher insertion loss at another operating frequency. Therefore, as a result, we successfully implemented a single-order diplexer in a PCB board.

CHAPTER 6

CONCLUSION

6.1 Conclusion

In this thesis, we successfully characterized crossed dipole antennas, and designed and implemented a diplexer based on a microstrip line and lumped elements. Although the implementation part only shows a small step in the diplexer design, we believe that, except for the expensive materials used in the application over ultra-high frequency (UHF), it is fully possible to design antennas and diplexers using regular materials (i.e. FR4, copper, etc.).

We observed that the behavior of the strip-dipole antenna can be replicated similarly to the behavior of the cylindrical antenna. Based on a previously found result [2], we can easily simulate the impedance of a strip dipole antenna by either analytical equations or circuit models. Moreover, different types of diplexer designs have been discussed in this thesis. Each design has its own advantage and disadvantage; thus, circuit design should pay attention to the tradeoffs in making the best choice. Chapter 5 provides an initial result of the possibility of constructing a diplexer on a small PCB. Since the usual diplexer design over the UHF range is large, the implementation part gave us confidence in designing a compact diplexer by lumped elements and microstrip lines.

6.2 Future Work

In the future, accomplishment of several implementation tasks is expected. Although we successfully designed a working diplexer based on single-order filter topology, there is still much room to improve it. We need to implement

a third-order filter and third-order diplexer to see if it can show a development of signal isolation without sacrificing too much insertion at the peak. Moreover, another goal for the future is to implement an effective matching network on the PCB. With the matching network, maximum power can be delivered from the antenna to the diplexer, and thus pass to the next RF module.

APPENDIX A

TEM-MODE TRANSMISSION LINE

The key difference between circuit theory and transmission line theory is electrical size [9]. For transmission lines whose lengths are much less than a wavelength of the transmitted signals, the lines can be evaluated by the basic voltage and current theory. However, as the frequency increases and the wavelength decreases, a complete electromagnetic solution called distribution circuit theory is needed to fully analyze the line structures. Electrical and magnetic field theory as associated with the TEM mode transmission line is very well established and well known.

Figure A.1 shows the equivalent circuit model of uniform transmission lines. There are usually four main physical entities associated with such a transmission line structure, which can be defined as follows.

R = series resistance per unit length, for both conductors, in Δ/m.

L = series inductance per unit length, for both conductors, in H/m.

G = shunt conductance per unit length, in S/m.

C = shunt capacitance per unit length, in F/m.

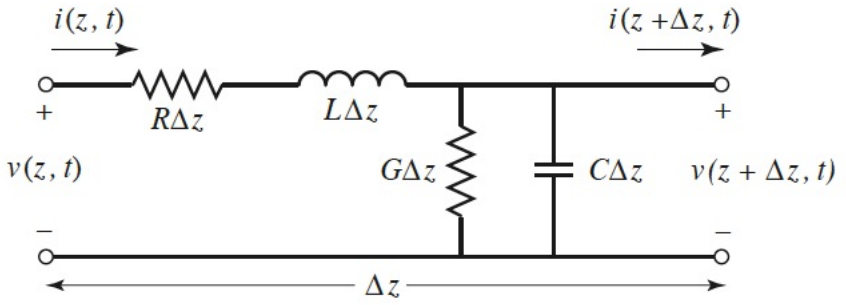

Figure A.1: Lumped-element equivalent circuit for transmission line

In most high-frequency transmission line structures, L and C tend to dominate because of the relatively high inductive reactance and capacitive susceptance. Therefore, in such situations, it is appropriate to assume the line to be approximately "loss-free".

The wave propagation along the TEM-mode transmission line can be characterized by the complex propagation constant as follows:

$$\gamma = \sqrt{(R + j\omega L)(G + j\omega C)} \tag{A.1}$$

The propagation constant can also be written as:

$$\gamma = \alpha + j\beta \tag{A.2}$$

When the loss-free approximation takes effect, Equation (A.2) is also equivalent to the following:

$$\beta = \omega\sqrt{LC} \tag{A.3}$$

We can also represent the propagation constant as:

$$\beta = \frac{2\pi}{\lambda} \tag{A.4}$$

From the relationship for phase velocity $v_p = f\lambda$, we can also write

$$v_p = \frac{\omega}{\beta} = \frac{1}{\sqrt{LC}} \tag{A.5}$$

Therefore, the review of TEM-mode transmission is sufficient to understand the content of this thesis.

APPENDIX B

CALIBRATION

In this chapter we will briefly discuss the procedure of calibrating the PCB board before measurement. The instrument we use to measure the PCB board is called a vector network analyzer (VNA). Network analyzers are very important measurement units for characterizing the performance of devices operating at high frequency. A network analyzer usually has two ports, one to send the incident signals and to measure the signals reflected back from the device, and the other to measure signals transmitted through the device. The block diagram of VNA, which is adapted from Agilent AN 1287-2, is shown in Figure B.1. Before measuring the PCB board, a calibration step is needed. There are two commonly used calibration methods: SOLT and TRL. We will briefly discuss the concept of calibration.

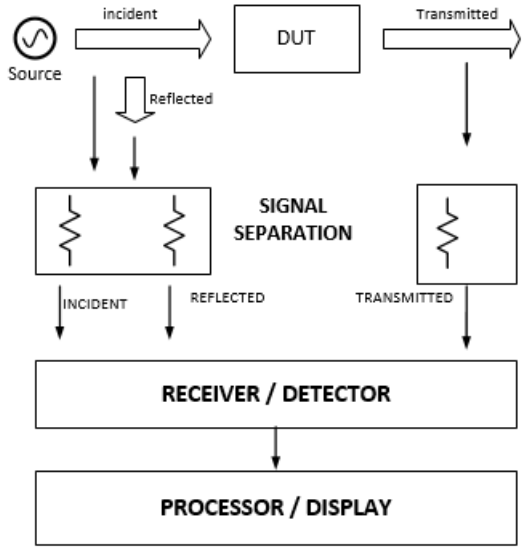

Figure B.1: Network analyzer block diagram

B.1 SOLT vs. TRL

In high-frequency measurement, it is usually difficult to connect devices to measurement ports directly. Therefore, measurement cables are always required for such measurement. However, cables, connectors and adapters can easily bring additional discontinuities, such as unwanted loss and reflection. Therefore, we need calibration to cancel such discontinuities.

When performing high-frequency measurement, it is important to designate the physical point where the measurement is taken, which is where the measurement plane is. For instance, if we make the calibration by placing the standards at the ends of the cables, then the reference planes will be at the ends of the cables. Figure B.2 shows a high-frequency model, where the Device Under Test represents the device we want to measure, A and B stand for measurement cables. Box X models the coupling between two ports, and it is usually ignored since it has little effect.

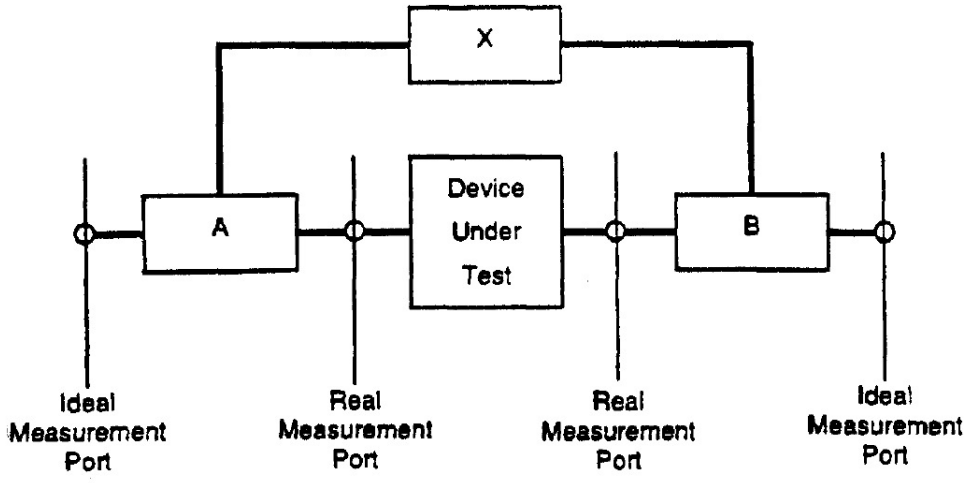

Figure B.2: Model for high-frequency measurement (adapted from [11])

The most common type of calibration used in coaxial systems is the SOLT calibration, which uses a Short, Open, matched Load, and a Thru as the known standards. Usually in SOLT calibration, such coaxial standards are very accurate and it is perfect to use them in coaxial systems. However, SOLT calibration is not very useful in the microstrip environment because Short, Open and Load standards are difficult to fabricate in microstrip. Moreover, the coaxial-to-microstrip transition on the edge of our PCB boards, which

introduces lots of discontinuities, cannot be accounted for in a SOLT calibration. Therefore, we use another calibration technique, TRL (Thru, Reflect and Load), because this calibration method uses microstrip lines as standards. The layout of a typical TRL standard is shown in Figure B.3.

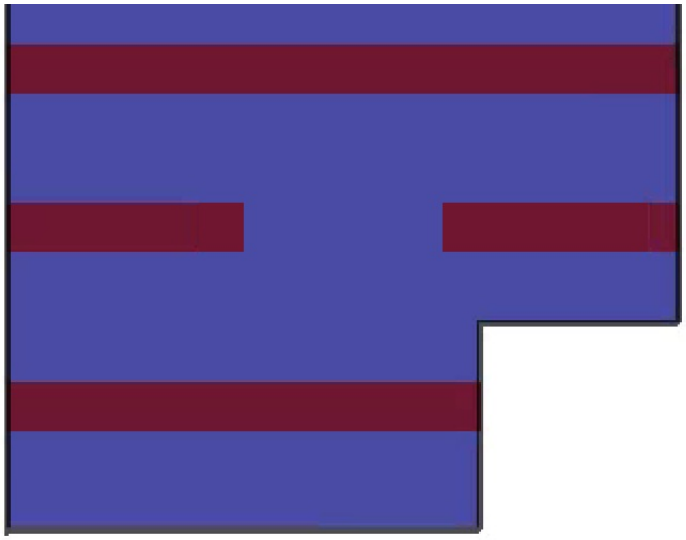

Figure B.3: Layout for TRL standards

The two separated lines in the middle are a Reflect standard, which usually has an open or short terminal in the end. The shorter line on the bottom represents a Thru standards, whose length is equal to the total length of the two Thru standards. The longer line on the top is a Line standard, whose length is the length of Thru plus the spacing between two Reflect standards. With the TRL calibration, the measurement plane is moved to the end of two Reflect standards.

REFERENCES

[1] S. Minin, "CubeSat Internal Documentation," unpublished.

[2] "Dipole antenna," 2016. [Online]. Available: https://en.wikipedia.org/wiki/Dipole˙antenna

[3] S. Keyrouz, H. J. Visser, and A. G. Tijhuis, "Novel empirical equations to calculate the impedance of a strip dipole antenna," *Radioengineering*, vol. 22, pp. 1258–1261, Dec. 2013.

[4] C. M. Bulter, "The equivalent radius of a narrow conducting strip," *IEEE Transaction on Antennas and Propagations*, vol. 30, pp. 755–758, 1982.

[5] R. S. Elliot, *Antenna Theory and Design*. Prentice Hall, 1981.

[6] B. Y. Toh, R. Cahill, and V. F. Fusco, "Understanding and measuring circular polarization," *IEEE Transaction on Education*, vol. 46, no. 3, pp. 313–318, Aug. 2003.

[7] M. Hamid and R. Hamid, "Equivalent circuit of dipole antenna of arbitrary length," *IEEE Transaction on Antennas and Propagations*, vol. 45, no. 11, pp. 1695–1696, Nov. 1997.

[8] "Diplexer," 2013. [Online]. Available: http://www.microwaves101.com/encyclopedias/diplexers

[9] D. M. Pozar, *Microwave Engineering*. Amherst, MA: John Wiley and Sons,Inc., 2012.

[10] S. Franke, *Wireless Communication Systems*. Class notes for ECE 453, Department of Electrical and Computer Engineering, University of Illinois at Urbana-Champaign, 2008.

[11] *Microwave Circuit Design Using Scattering Parameters*. Class notes for ECE 447, Department of Electrical and Computer Engineering, University of Illinois at Urbana-Champaign, Professor Milton Feng, 2009.